Supporting Information

Effects of Proton Tunneling Distance on CO_2 Reduction by Mn Terpyridine Species

Yuhang Qing,[a] Qianqian Wu,[a] Shuanglin He,[a] Ping Zhang,[a] Ying Xiong,[a] Yaping Zhang,[a] Fang Huang,[b] Fei Li[,c] and Lin Chen*[,a]*

[a] State Key Laboratory of Environment-Friendly Energy Material, School of Materials and Chemistry, Southwest University of Science and Technology, Mianyang 621010, P. R. China

[b] College of Chemistry, Chemical Engineering and Materials Science, Shandong Normal University, Jinan 250014, P. R. China

[c] State Key Laboratory of Fine Chemicals, Dalian University of Technology, Dalian 116024, P. R. China

Corresponding Authors

Email*: chenlin101101@aliyun.com

Email*: fanghuang@sdnu.edu.cn

Email*: lifei@dlut.edu.cn

Contents

1. Figure Contents

2. Table Contents

3. Scheme Contents

4. Materials and Instruments

All manipulations for preparation and handling of organometallic complexes were carried out under air. All the solvents were used as received. Other commercially available chemicals such as $Mn(CO)_5Br$, $Pd(PPh_3)_4$, benzaldehyde, 1-(pyridin-2-yl)ethanone, potassium hydroxide, pyridine，Toluene, potassium carbonate, anhydrous methanol and iodine were purchased from local suppliers and used as received. Water was deionized with the Millipore Milli-Q UF Plus system. Glass carbon disc (3 mm), Ag^+/Ag electrode and platinum wire were purchased from CHI for electrochemical studies.

NMR Spectra were collected with a varian INOVA 600 NMR spectrometer. Mass spectra were recorded with HP 1100 HPL/ESI-DAD-MS and Waters/Micromass LC/Q-TOF-MS instruments. Elemental analyses were performed with a Thermoquest-Flash EA 1112 elemental analyzer.

5. Crystallographic Structure Determinations

The single-crystal X-ray diffraction data were collected with an Bruker Smart Apex II CCD diffractometer with agraphite-monochromated Mo-*K* radiation (= 0.071073 Å) at 100 K using the θ-2 scan mode. Data processing was accomplished with the SAINT processing program. Intensity data were corrected for absorption by the SADABS program. All structures were solved by direct methods and refined on F^2 against full-matrix least-squares methods by using the SHELXTL 97 program package. All non-hydrogen atoms were refined anisotropically. Hydrogen atoms were located by geometrical calculation. Crystallographic data and selected bond lengths and angles for **1p** are given in Tables S1–S3. **CCDC-2038280** contain the supplementary crystallographic data for this paper. These data can be obtained free of charge from The Cambridge Crystallographic Data Centre via http://www.ccdc.cam.ac.uk/data_request/cif.

Table S 1 Bond lengths [Å] for **1p**

Atom	Atom	Length/Å	Atom	Atom	Length/Å
Br1	Mn1	2.4367(12)	C9	C10	1.394(8)
Mn1	N3	2.085(4)	C10	C11	1.388(7)
Mn1	N4	2.039(4)	C11	C12	1.490(7)
Mn1	C28	1.797(6)	C12	C13	1.376(7)
Mn1	C29	1.781(6)	C13	C14	1.402(8)
Mn1	C30	1.810(5)	C14	C15	1.391(8)
O1	C31	1.230(6)	C14	C17	1.485(8)
O2	C30	1.152(6)	C15	C16	1.377(8)
O3	C29	1.162(6)	C16	C23	1.477(8)
O4	C28	1.151(7)	C17	C18	1.400(9)
N1	C1	1.426(6)	C17	C22	1.338(10)
N1	C31	1.352(6)	C18	C19	1.407(11)
N2	C7	1.341(6)	C19	C20	1.411(15)
N2	C11	1.342(7)	C20	C21	1.350(14)
N3	C12	1.361(6)	C21	C22	1.392(10)
N3	C16	1.363(6)	C23	C24	1.397(7)
N4	C23	1.346(7)	C24	C25	1.402(10)
N4	C27	1.339(7)	C25	C26	1.350(11)
C1	C2	1.403(7)	C26	C27	1.376(8)
C1	C6	1.366(8)	C31	C32	1.503(7)
C2	C3	1.384(7)	C32	C33	1.383(7)
C2	C7	1.467(8)	C32	C37	1.398(7)
C3	C4	1.381(9)	C33	C34	1.389(8)

C4	C5	1.377(9)	C34	C35	1.368(7)
C5	C6	1.375(8)	C35	C36	1.372(8)
C7	C8	1.417(7)	C36	C37	1.394(8)
C8	C9	1.356(9)			

Table S 2 Bond Angle for **1p**

Atom	**Atom**	**Atom**	**Angle/°**	**Atom**	**Atom**	**Atom**	**Angle/°**
N3	Mn1	Br1	85.92(12)	C10	C11	C12	119.5(5)
N4	Mn1	Br1	88.89(12)	N3	C12	C11	119.3(4)
N4	Mn1	N3	78.63(17)	N3	C12	C13	123.0(5)
C28	Mn1	Br1	91.42(18)	C13	C12	C11	117.7(5)
C28	Mn1	N3	171.5(2)	C12	C13	C14	120.7(5)
C28	Mn1	N4	93.3(2)	C13	C14	C17	122.7(6)
C28	Mn1	C30	85.8(2)	C15	C14	C13	115.9(5)
C29	Mn1	Br1	174.36(16)	C15	C14	C17	121.4(6)
C29	Mn1	N3	92.5(2)	C16	C15	C14	121.1(5)
C29	Mn1	N4	96.1(2)	N3	C16	C15	122.8(5)
C29	Mn1	C28	90.9(2)	N3	C16	C23	114.6(5)
C29	Mn1	C30	90.5(2)	C15	C16	C23	122.6(5)
C30	Mn1	Br1	84.53(16)	C18	C17	C14	119.0(6)
C30	Mn1	N3	101.98(19)	C22	C17	C14	121.3(6)
C30	Mn1	N4	173.3(2)	C22	C17	C18	119.7(6)
C31	N1	C1	129.1(5)	C17	C18	C19	118.5(9)
C7	N2	C11	119.7(4)	C18	C19	C20	120.0(10)
C12	N3	Mn1	128.9(3)	C21	C20	C19	119.5(8)
C12	N3	C16	116.4(4)	C20	C21	C22	119.9(10)
C16	N3	Mn1	114.5(4)	C17	C22	C21	122.3(9)
C23	N4	Mn1	116.5(3)	N4	C23	C16	115.0(4)
C27	N4	Mn1	125.2(4)	N4	C23	C24	122.5(6)
C27	N4	C23	118.0(5)	C24	C23	C16	122.5(5)
C2	C1	N1	118.7(5)	C23	C24	C25	117.0(6)
C6	C1	N1	121.1(5)	C26	C25	C24	120.5(6)
C6	C1	C2	120.1(5)	C25	C26	C27	118.8(7)
C1	C2	C7	125.2(5)	N4	C27	C26	123.1(7)
C3	C2	C1	116.9(5)	O4	C28	Mn1	177.8(5)
C3	C2	C7	117.8(5)	O3	C29	Mn1	178.0(4)
C4	C3	C2	123.1(6)	O2	C30	Mn1	172.9(5)
C5	C4	C3	118.4(6)	O1	C31	N1	123.5(5)
C6	C5	C4	119.9(7)	O1	C31	C32	119.9(5)

C1	C6	C5	121.6(6)	N1	C31	C32	116.5(5)
N2	C7	C2	119.5(4)	C33	C32	C31	123.5(4)
N2	C7	C8	119.5(5)	C33	C32	C37	119.6(5)
C8	C7	C2	121.1(5)	C37	C32	C31	116.8(5)
C9	C8	C7	120.7(5)	C32	C33	C34	119.3(5)
C8	C9	C10	119.5(5)	C35	C34	C33	121.7(6)
C11	C10	C9	117.5(6)	C34	C35	C36	119.1(6)
N2	C11	C10	123.2(5)	C35	C36	C37	120.9(5)
N2	C11	C12	117.3(4)	C36	C37	C32	119.4(6)

Symmetry transformations used to generate equivalent atoms:

Table S 3 Crystal data and structure refinement for **1p**.

Identification code	exp_2211
Empirical formula	$C_{74}H_{48}BrMn_2N_8O_8$
Formula weight	1366.99
Temperature/K	99.9(3)
Crystal system	monoclinic
Space group	$P2_1/c$
a/Å	12.2992(7)
b/Å	16.1840(10)
c/Å	19.0169(12)
α/°	90
β/°	108.760(7)
γ/°	90
Volume/Å^3	3584.2(4)
Z	2
ρ_{calc}g/cm^3	1.267
μ/mm^{-1}	0.967
F(000)	1394.0
Crystal size/mm^3	0.12 × 0.11 × 0.1
Radiation	Mo Kα (λ = 0.71073)
2Θ range for data collection/°	4.308 to 49.998
Index ranges	-14 ≤ h ≤ 14, -19 ≤ k ≤ 15, -18 ≤ l ≤ 22
Reflections collected	23945
Independent reflections	6323 [R_{int} = 0.1135, R_{sigma} = 0.1084]
Data/restraints/parameters	6323/0/424
Goodness-of-fit on F^2	1.029
Final R indexes [I>=2σ (I)]	R_1 = 0.0773, wR_2 = 0.1958
Final R indexes [all data]	R_1 = 0.1169, wR_2 = 0.2282
Largest diff. peak/hole / e Å^{-3}	0.99/-0.47

6. Electrochemistry Study Details

Cyclic voltammetry (CV): Cyclic voltammetry experiments were carried out in a three-electrode cell under high-purity Ar (99.999%) or CO_2 (99.99%) using CHI 760E potentiostat. The working electrode was a glassy carbon disc (diameter 3 mm) polished with 0.5-mm diamond pastes, then sonicated in ion-free water for 15 min and washed with MeCN prior to use. The reference electrode was a Ag^+/Ag (0.01 M $AgNO_3$) electrode and the counter electrode was platinum wire. Manganese complex concentrations were generally at 0.5 mM. A solution of 0.1 M $^nBu_4NPF_6$ (Fluka, electrochemical grade) in CH_3CN was used as supporting electrolyte, which was degassed by bubbling with dry Ar or CO_2 for 5 min before measurement. The catalytic experiments with CO_2 were performed in CO_2-saturated CH_3CN solution (about 0.28 M) with addition of a certain amount of anhydrous PhOH. The scan rate is 100 mV/s. Ferrocene (Fc) was added as an internal reference in the end of each measurement to convert the measured potentials and ***all potentials given in this work are referred to*** $Fc^{+/0}$.

Controlled potential electrolysis experiments (CPE)： Controlled potential electrolysis experiments were carried out in a custom 18 mL cell designed in our laboratory. The setup included a glassy carbon cell working electrode, graphite rod counter electrode separated from the solution by a porous glass frit, and $Ag/AgNO_3$ pseudoreference electrode. For the catalytic electrolysis studies, the cell was charged with Mn catalyst (0.5 mM) and PhOH (1 M) in 0.1 M $^nBu_4NPF_6$ solution (CH_3CN). Gas products were quantified by analyzing 50 μL aliquots of the headspace on a Beifen 6890A Series gas chromatograph. The partial pressure of H_2/CO in the headspace was determined by comparison to gas standard samples. Henry's Law was used to calculate the total H_2/CO production, given as the sum of headspace and dissolved H_2/CO.

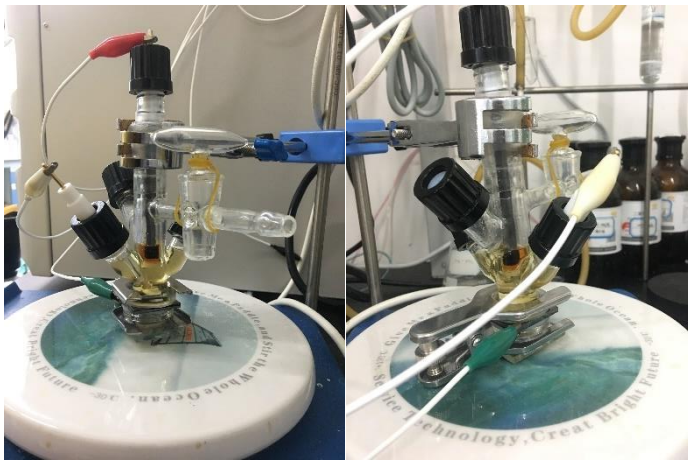

Typical Experimental Conditions:

Purity of the electrolyte medium was confirmed over the available electrochemical window through background scans taken prior to addition of analyte. 2.9 mg (0.5 mM) of **1p** and 0.74 g (1 M) of PhOH were weighed into an 18 mL glass vial and dissolved in 8 mL of a supporting electrolyte solution (0.1 M $[^{n}Bu_4N][PF_6]/CH_3CN$). The solution was saturated with CO_2 by bubbling CO_2 into the electrolyte for about 30 min prior to the experiment.

7. Product Analysis

The **gas products** in the headspace of the cell were analyzed by a gas chromatograph (GC, Beifen 6890A s), which was equipped with TCD and FID detectors. Gas sample H_2, CH_4 and CO are separated by stainless-steel column packed with molecular sieves (5 Å ×3 m) and the carrier gas is Ar (flow rate = 35 mL min^{-1}). The TCD detector was used to detect H_2 at a detection limit of 1 ppm. The FID detector was furnished with a methanizer to detect CH_4 and CO at a detection limit of 0.5 ppm. Gas chromatography calibration curves were made by sampling known volumes of H_2, CH_4 and CO gas. Other gas samples such as ethyene and ethanal could be separated by Porapak N column and detected by FID. The operating temperatures of the injection port, the oven/column, and detector were 50°C, 50°C and 380°C, respectively. Aliquots (50 μL) of the gas headspace were injected into the GC in the end of electrolysis to analyze the gas products formed. The gas path is shown in the figure below.

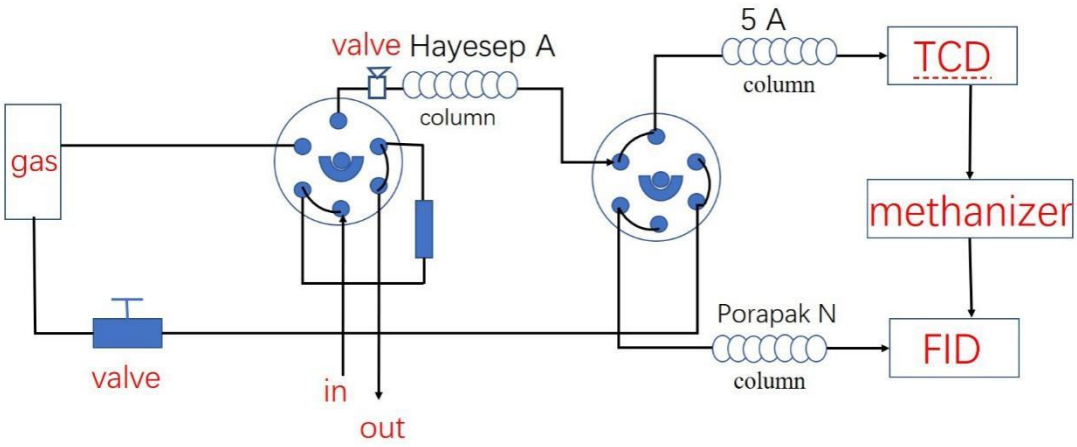

The **liquid product** (HCOOH) in the resulting electrolyte was detected by using ion chromatograph (Shenghan ICS-380), which was equipped with an electrical conductivity detector and an ionic exchange column. The ion chromatographic measurements were made with 1 M K_2CO_3/$KHCO_3$ aqueous solution as flowing phase in a negative ion model and with potassium formate as external stantard. Before measurement, the resulting electrolyte was treated with 1 M K_2CO_3/$KHCO_3$ aqueous solution for 1 h to convert formic acid in the solution to potassium formate.

8. Calculation for Faradaic Efficiency

$$Faradaic\ yield\ product\ (\%) = 100 \times n_{prod}./\ (Q / F / 2)$$

Where F is the Faraday constant (C mol^{-1}), n_{prod} (mol) is the amount of CO measured in the headspace, and Q (C) is the charged passed during electrolysis.

9. Fourier-Transform Infrared Reflectance Spectroelectrochemistry (FTIR-SEC)

A homemade FTIR-SEC instrument was used for this study. The cell consists of a glass carbon working electrode (10 mm), a Pt counter (15 mm × 30 mm) electrode, and a $Ag/AgNO_3$ reference electrode and a CaF_2 plate as the optical window. The IR beam is directed to focus on the working electrode through the optical window, where it is reflected and ultimately directed to the Bruker Vertex 80 detector. The dry CH_3CN solution (0.2 M TBAP) prepared under an atmosphere of Ar is used as the electrolyte.

10. Experiment section

General procedure for the preparation of the target ligands involved in this article. The procedure was slightly modified according to the literature (Solan, G. A. et. al. Organometallics 2013, 32, 249−259). An oven-dried Schlenk flask equipped with a stir bar was evacuated, back-filled with Ar, and charged with 1 equiv 2-bromo-precursors, 1.1 equiv corresponding phenylboric acid, 0.05 equiv $Pd(PPh_3)_4$, toluene (50 mL), ethanol (50 mL) and an aqueous 2 M solution of potassium carbonate (12 mL). The solution was stirred at room temperature for 15 min before heated to 90 °C for 42 h, the mixture was cooled to room temperature and 30% hydrogen peroxide (0.4 mL) was added. The mixture was stirred at room temperature for 30 min, the product was extracted using diethyl ether (2 × 100 mL), and the extract was washed with saturated sodium chloride solution (1× 30 mL) and water (3 × 30 mL) to give a red organic layer. Following drying with magnesium sulfate, the volatiles were removed under reduced pressure to give an orange-brown residue. The catalyst residues were removed using a short silica gel column employing dichloromethane as eluting solvent. After the solvent was removed under reduced pressure, the product was obtained as a solid.

Synthesis of ligand L^1

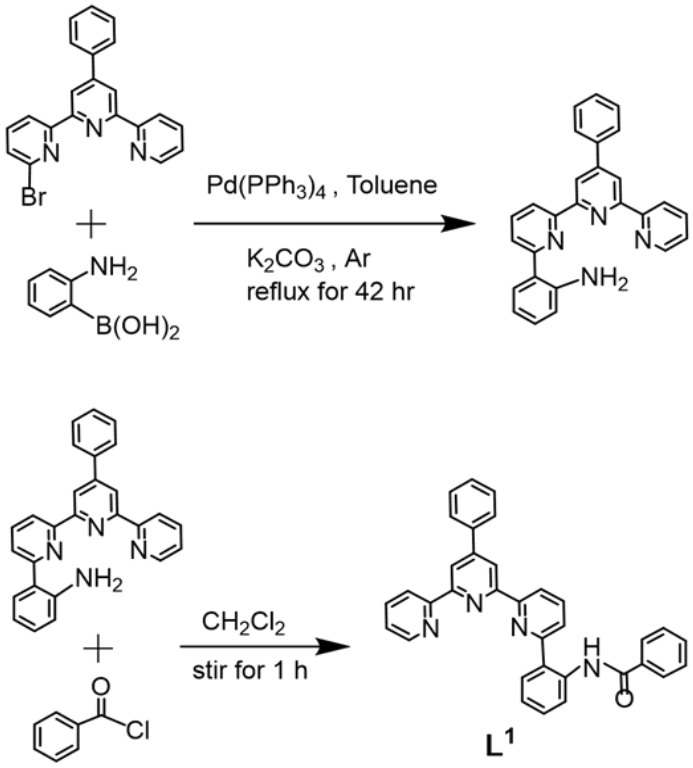

Scheme S 1 preparation of target ligands $\mathbf{L^1}$

2-bromo-6-(4-phenyl-6-(pyridin-2-yl)pyridin-2-yl)pyridine was obtained according to literature procedures. (Constable, E. C. *et. al. J. Chem. Soc., Dalton Trans*., **1996**, *389*, 4207-4216). 2-(6-(4-phenyl-6-(pyridin-2-yl)pyridin-2-yl)pyridin-2-yl)aniline, which was obtained according to literature procedures (Solan, G. A. et. al. *Organometallics*., **2013**, *32*, 249−259).

Preparation of $\mathbf{L^1}$. $\mathbf{L^1}$ was prepared by stirring the mixture of benzoyl chloride and 2-(6-(4-phenyl-6-(pyridin-2-yl)pyridin-2-yl)pyridin-2-yl)aniline. Excessive benzoyl chloride was added to a solution of 2-(6-(4-phenyl-6-(pyridin-2-yl)pyridin-2-yl)pyridin-2-yl)aniline (1 g, 2.5 mmol) in CH_2Cl_2 (15 ml). The triethylamine (3-5 ml) was added to the mixture after 5 minutes. The resulting mixture was stirred at room temperature for 1 h. Finally, the mixture was poured into weak base solution for dispose of the excessive benzoyl chloride. The mixture solution was extracted with CH_2Cl_2 (3×50 ml). The product was purified by column chromatograph (CH_2Cl_2) over silica gel to obtain $\mathbf{L^1}$. ^{1}H NMR (DMSO, 600 MHz): δ 11.92 (1H, s), 9.13~9.05 (3H, m), 8.95 (1H, s), 8.75~8.72 (1H, t), 8.63 (1H, m), 8.38~8,37 (1H, d), 8.27~8.24 (1H, t), 8.15~8.13 (1H, t), 8.05~8.03 (1H, d), 7.91~7.90 (1H, d), 7.78~7.77 (2H, d), 7.62~7.53 (3H, m), 7.51~7.50 (3H, m), 7.40~7.38 (1H, t),

7.23~7.21 (1H, t), 6.96~6.94 (2H, t). ESI-MS: Calcd for $[M+H^+]^+$: *m/z* 505.58; found: 505.20.

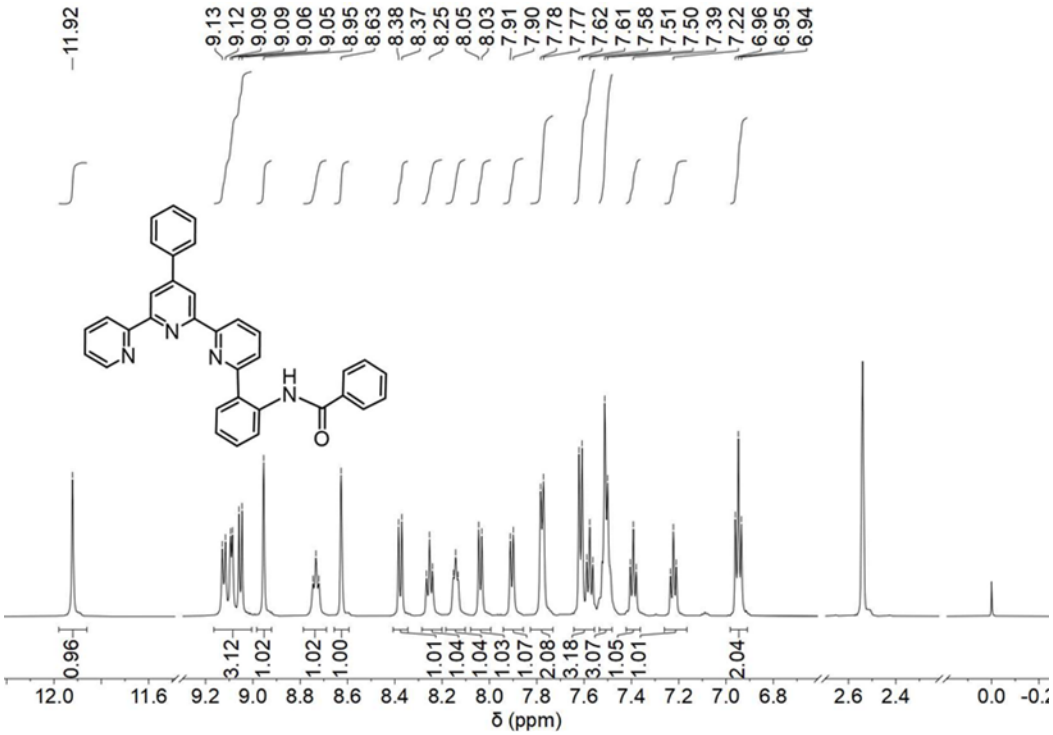

Figure S 1 ^{1}H NMR (DMSO, 600 MHz) spectrum of **L^1**.

Synthesis of ligand L^2

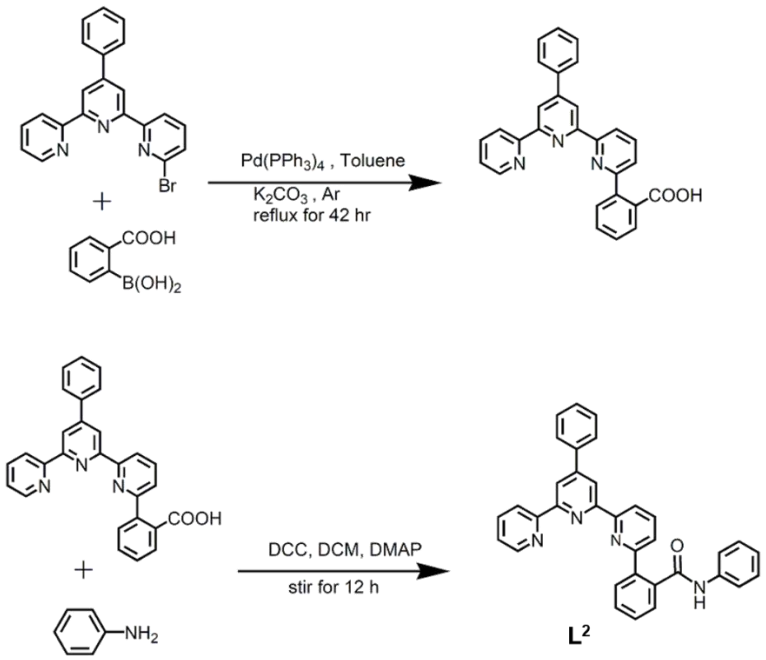

Scheme S 2 preparation of target ligands **L^2**

2-bromo-6-(4-phenyl-6-(pyridin-2-yl)pyridin-2-yl)pyridine was obtained according to literature procedures. (Constable, E. C. *et. al. J. Chem. Soc., Dalton Trans*., **1996**, *389*, 4207-4216). 2-(6-(4-phenyl-6-(pyridin-2-yl)pyridin-2-yl)pyridin-2-yl)benzoic acid was obtained according to literature procedures (Solan, G. A. et. al. *Organometallics*., **2013**, *32*, 249−259).

Preparation of **L²**. 2-(6-(4-phenyl-6-(pyridin-2-yl)pyridin-2-yl)pyridin-2-yl)benzoic acid (1.72 g, 4 mmol) was dissolved in CH_2Cl_2 (15 ml) and dicyclohexylcarbodiimide (DCC, 1.65 g, 8 mmol) was added. Aniline (0.75 g, 8 mmol) and 4-dimethylaminopyridine (0.1 g, 8 mmol) was added after the mixture stirred for 10 minutes. Then the mixture was stirred for 12 h. Finally, the product was purified by low temperature filtration. Evaporation of the solvent, the product was purified by column chromatograph (CH_2Cl_2) over silica gel to obtain **L²**. ^{1}H NMR (DMSO, 600 MHz): δ 10.29 (1H, s), 8.75 ~ 8.74 (2H, m), 8.65~8.60 (3H, m), 8.14~8.11 (1H, t), 8.03 (1H, t), 7.91~7.87 (2H, m), 7.81~7.80 (2H, d), 7.67~7.65 (2H, m), 7.62~7.60 (1H, m), 7.56~7.51 (4H, m), 7.44~7.43 (2H, m), 6.91~6.88 (2H, t), 6.78~6.75 (1H, t). ESI-MS: Calcd for $[M+H^+]^+$: *m/z* 505.22; found: 505.41.

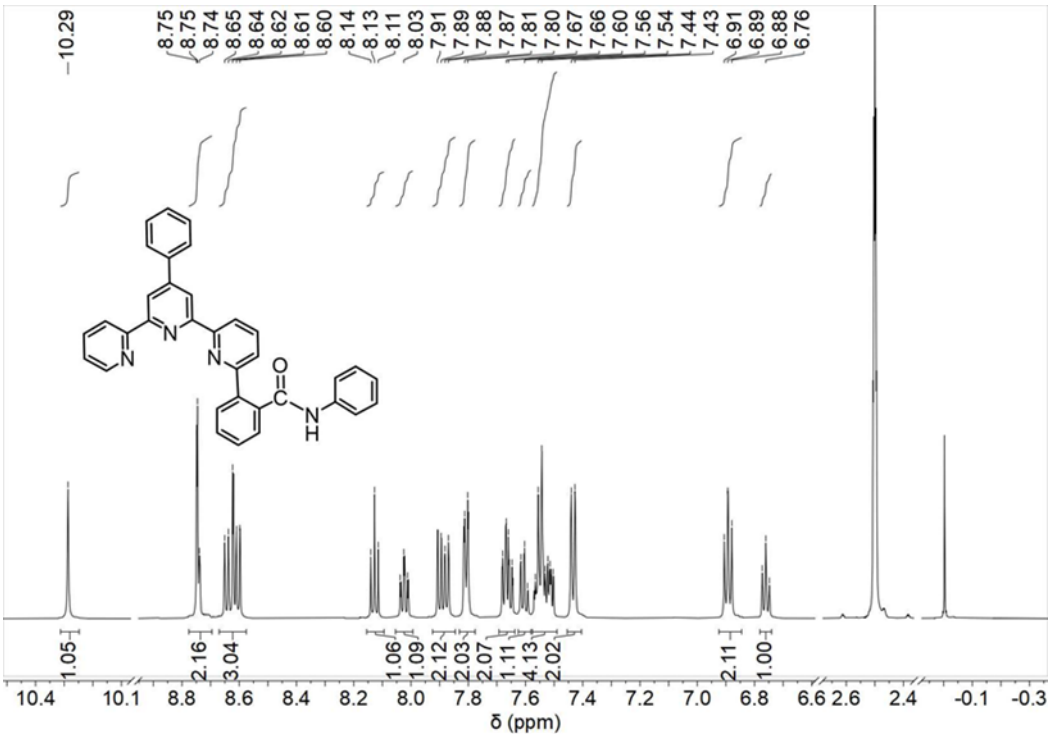

Figure S 2 ^{1}H NMR (DMSO, 600 MHz) spectrum of **L²**.

Synthesis of ligand L^3

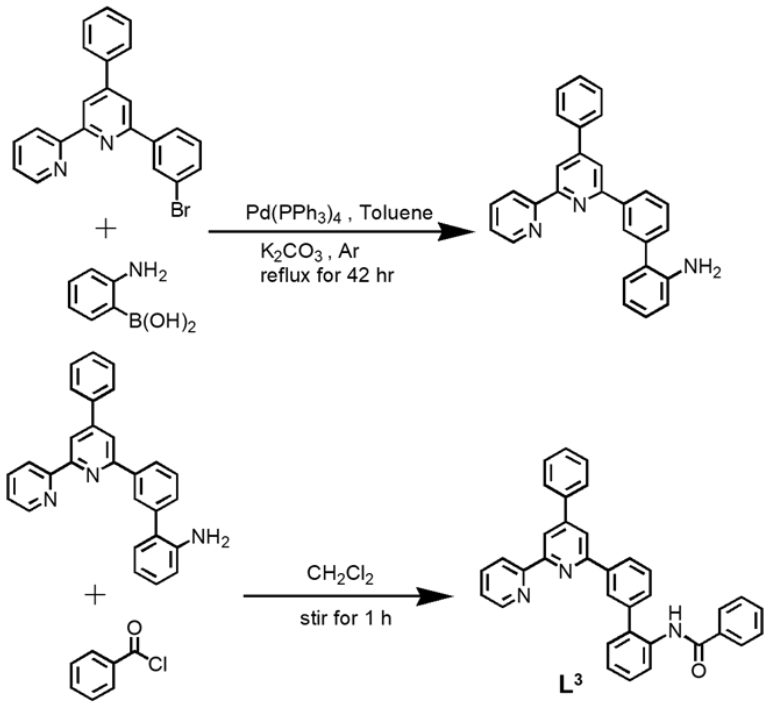

Scheme S 3 preparation of target ligands L^3

2-bromo-6-(4-phenyl-6-(pyridin-2-yl)pyridin-2-yl)phenyl was obtained according to literature procedures. (Constable, E. C. *et. al. J. Chem. Soc., Dalton Trans*., **1996**, *389*, 4207-4216).

Preparation of L^3. L^3 was prepared by stirring the mixture of benzoyl chloride and 2-(6-(4-phenyl-6-(pyridin-2-yl)pyridin-2-yl)phenyl-2-yl)aniline, which was obtained according to literature procedures (Solan, G. A. et. al. Organometallics 2013, 32, 249−259). The experimental procedure is the same with L^1. ^{1}H NMR ($DCCl_3$, 600 MHz): δ 8.71 (2H, s), 8.62~8.61 (1H, d), 8.56~8.55 (1H, d), 8.41 (1H, s), 8.27~8.26 (1H, s), 8.22 (1H, d), 8.02 (1H, s), 7.81~7.80 (3H, t), 7.69~7.67 (3H, m), 7.55~7.56 (1H, d), 7.53~7.50 (3H, m), 7.48~7.47 (1H, d), 7.44~7.43 (1H, m), 7.35~7.34 (2H, m), 7.30~7.27 (1H, t), 7.25~7.23 (1H, d). ESI-MS: Calcd for $[M+H^+]^+$: *m*/*z* 504.23; found: 504.59.

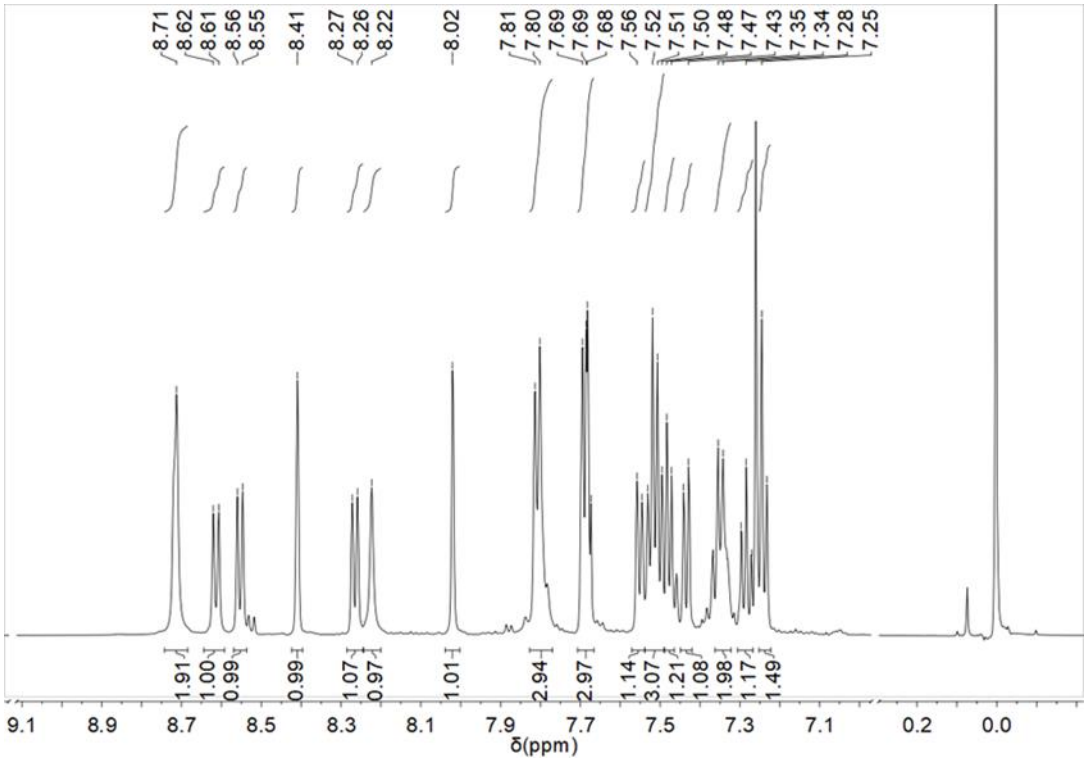

Figure S 3 ^{1}H NMR ($CDCl_3$, 600 MHz) spectrum of $\mathbf{L^3}$.

Synthesis of complexes 1p, 2p and 3

Synthesis of complex 1p

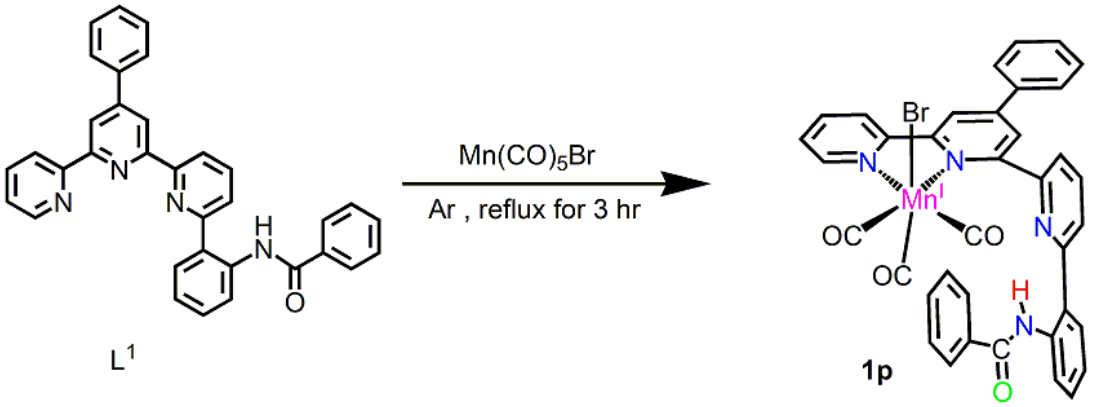

Scheme S 4 preparation of target complex **1p**

Preparation of 1p. Compound $Mn(CO)_5Br$ (0.2 g, 0.72 mmol) was added to a degassed methanol solution (20 mL) of L^1 (0.363 g, 0.72 mmol). The resulting orange solution was heated to reflux for 3 h under argon, then allowed to cool to room temperature before filtration. The filtrate was collected and concentrated, then washed with Et_2O and dried in vacuo to afford 0.42 g (85% yield) of orange product. The following were observed for the mixture of atropisomers (hydroxyphenyl adduct parallel and antiparallel to the axial plane): IR (THF) υ_{CO}: 2020(s), 1927(br)，1903(m) cm^{-1}. ^1H NMR (DMSO, 600 MHz): δ 12.68 (1H, s), 9.04~9.12 (3H, m), 8.52~8.53 (1H, d), 8.23~8.31 (6H, m), 8.05~8.08 (2H, m), 7.64~7.66 (4H, m), 7.48~7.51 (2H, m), 7.30~7.32 (3H, m), 6.82 (2H, s). Anal. Calcd for C37H24BrMnN4O4(%): C, 61.43; H, 3.34; N, 7.74. found: C, 61.45; H, 3.32; N, 7.75. MS (TOF-ES): m/z =643.1180 $[M–Br^-]^+$, m/z = 615.1229 $[M–Br^--CO]^+$.

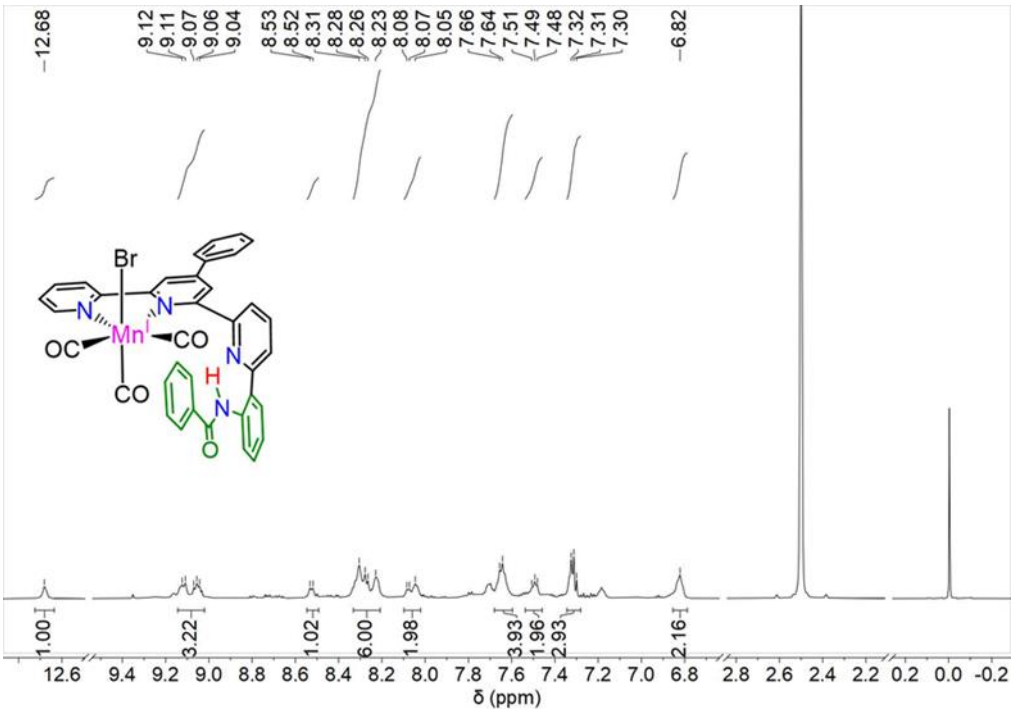

Figure S 4 ^{1}H NMR (DMSO, 600 MHz) spectrum of **1p**.

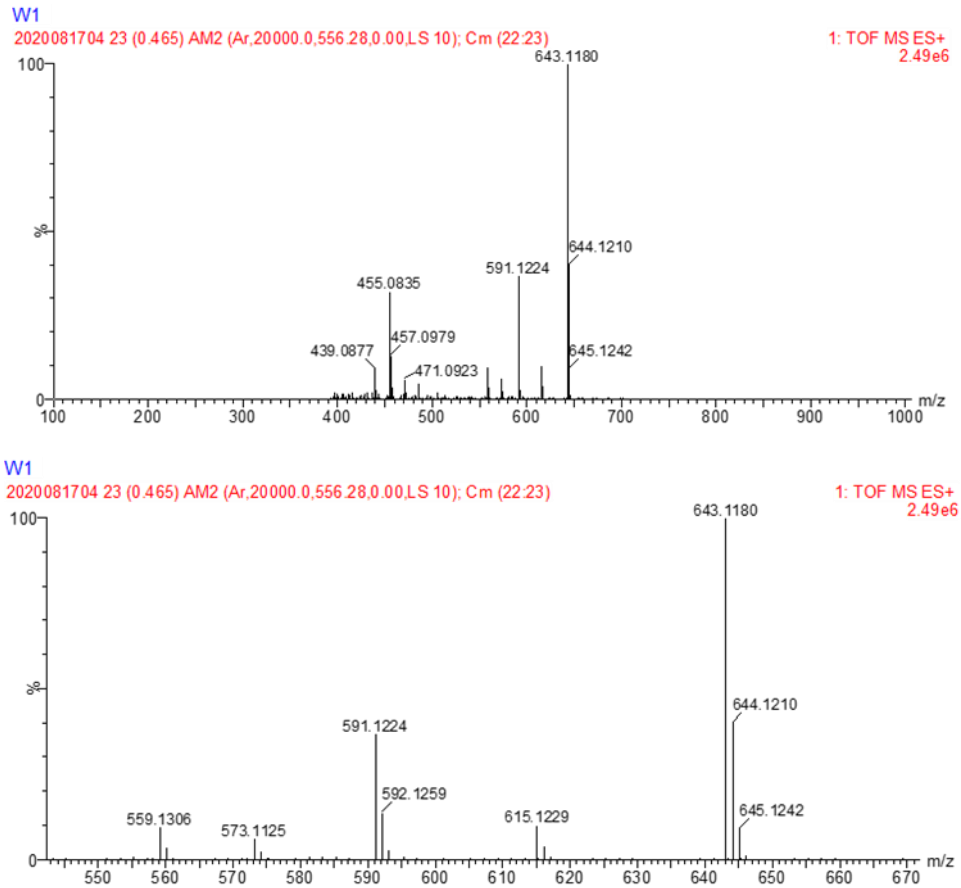

Figure S 5 High resolution mass spectra of complex **1p**.

Synthesis of complex 2p

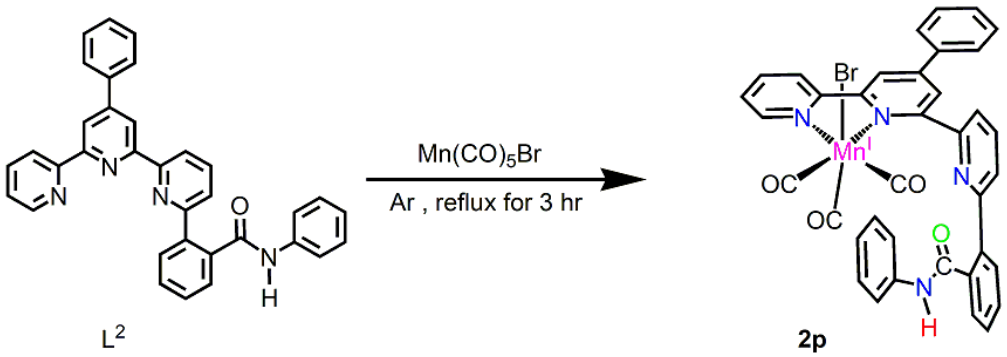

Scheme S 5 preparation of target complex **2p**

Preparation of 2p. Replacing ligand $\mathbf{L^1}$ with $\mathbf{L^2}$, complex **2p** was prepared by the same way with complex **1p** in a yield of 82%. IR (THF) ν_{CO} for complex **2p**: 2025 (s), 1932(br)， 1917 (m) cm^{-1}. ^1H NMR (DMSO, 600 MHz): δ 10.29 (1H, s), 9.20~9.21 (1H, d), 8.95~8.96 (1H, m), 8.91 (1H, s), 8.25 ~ 8.28 (1H, m), 8.11~8.13 (1H, m), 7.88~7.89 (2H, d), 7.71~7.80 (4H, m), 7.57~7.63 (8H, m), 6.89~7.05 (4H, m). Anal. Calcd for C37H24BrMnN4O4(%): C, 61.43; H, 3.34; N, 7.74. found: C, 61.50; H, 3.31; N, 7.70. MS (TOF-ES): m/z =643.1177 $[M–Br^-]^+$, m/z = 615.1226 $[M–Br^-\text{-}CO]^+$, m/z = 559.1309 $[M–Br^-\text{-}3CO]^+$.

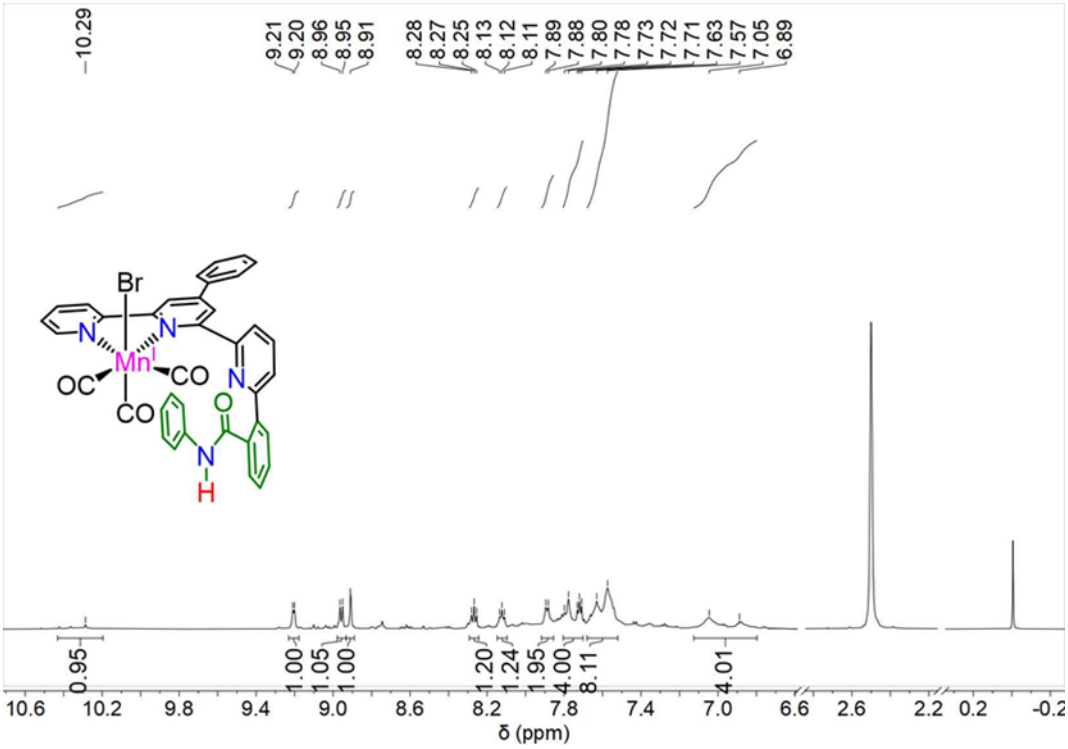

Figure S 6 ^1H NMR (DMSO, 600 MHz) spectrum of **2p**.

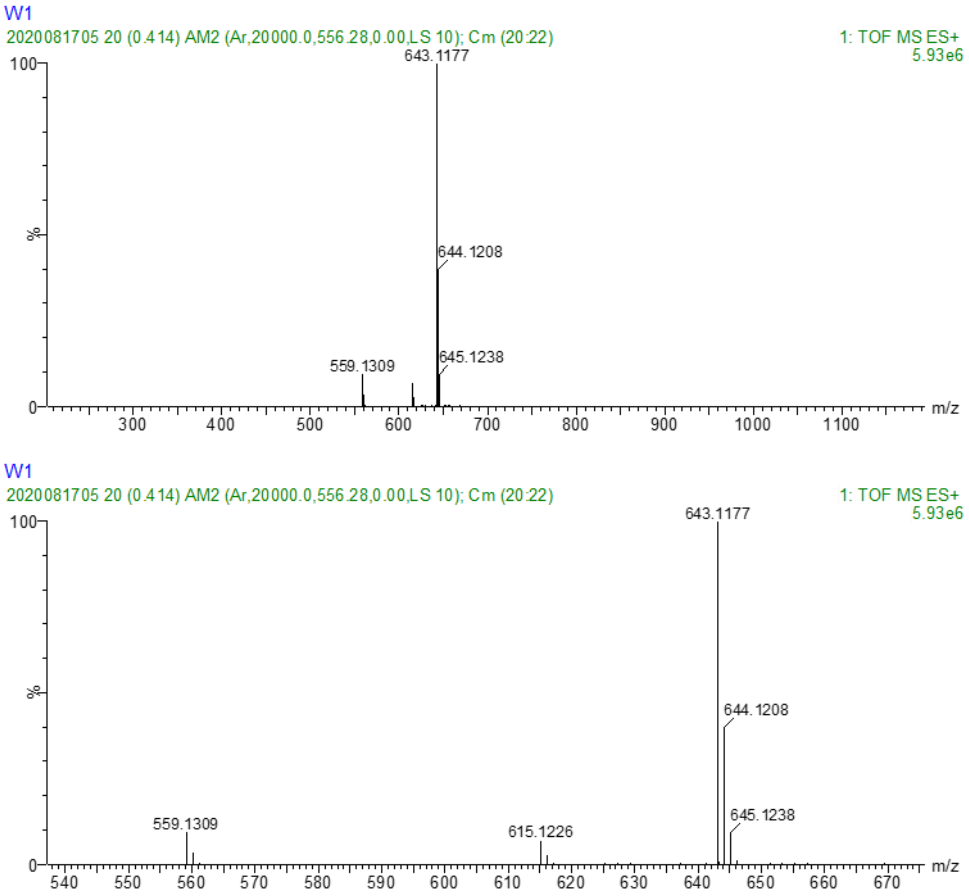

Figure S 7 High resolution mass spectra of complex **2p**.

Synthesis of complex 3

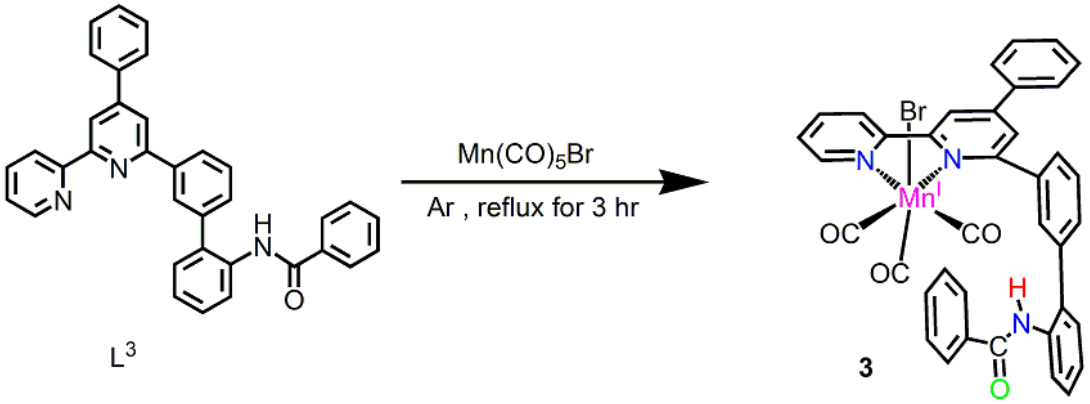

Scheme S 6 preparation of target complex **3**

Preparation of 3. Replacing ligand $\mathbf{L^1}$ with $\mathbf{L^3}$, complex **3** was prepared by the same way with

complex **1p** and **2p** in a yield of 88%. IR (THF) v_{CO} for complex **3**: 2026 (s), 1938 (br)，1912 (s) cm^{-1}. ^1H NMR (DMSO, 600 MHz): δ 9.21 (1H, s), 8.98~8.96 (1H, d), 8.94~8.92 (1H, d), 8.28~8.26 (1H, t), 8.05 (1H, s), 7.90~7.89 (1H, d), 7.83~7.82 (1H, d), 7.79 (1H, s), 7.73 (1H, t), 7.67 (2H, d), 7.62~7.60 (4H, m), 7.56~7.53 (2H, m), 7.48~7.44 (3H, m), 7.40~7.37 (2H, t), 7.31~7.30 (1H, d). Anal. Calcd for C38H25BrMnN3O4(%): C, 63.17; H, 3.99; N, 8.91. found:C, 63.20; H, 3.95; N, 8.90. MS (TOF-ES): m/z =642.1150 $[M–Br^-]^+$.

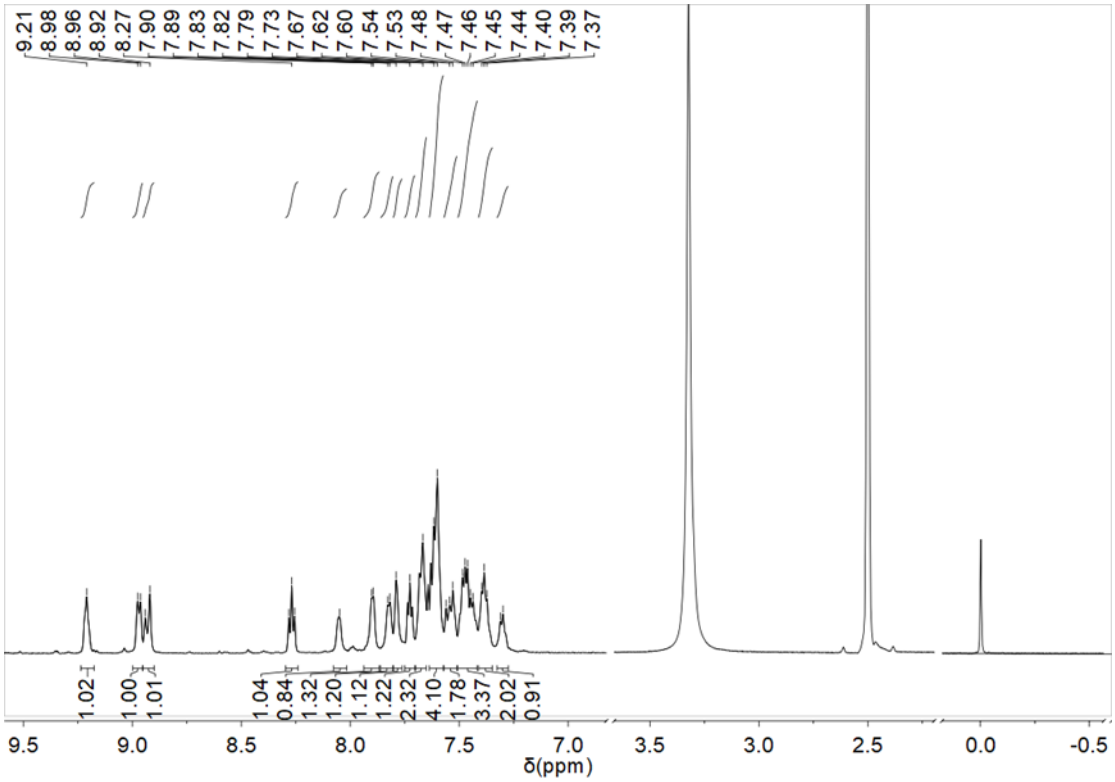

Figure S 8 ^1H NMR (DMSO, 600 MHz) spectrum of **3.**

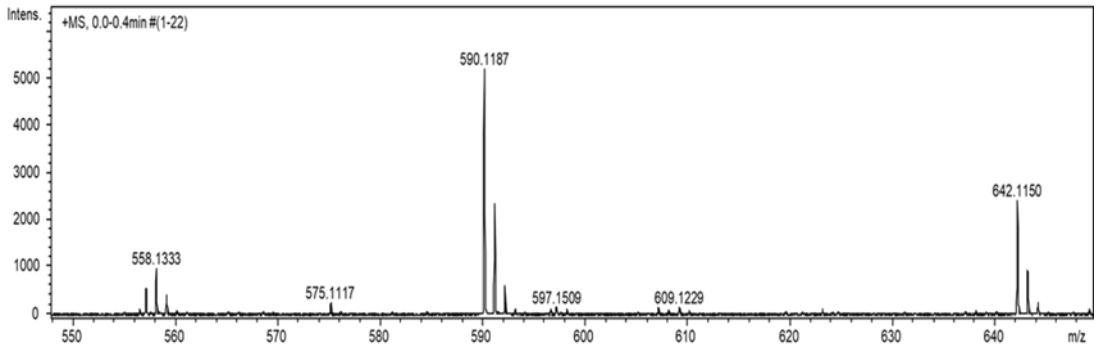

Figure S 9 High resolution mass spectra of complex **3**.

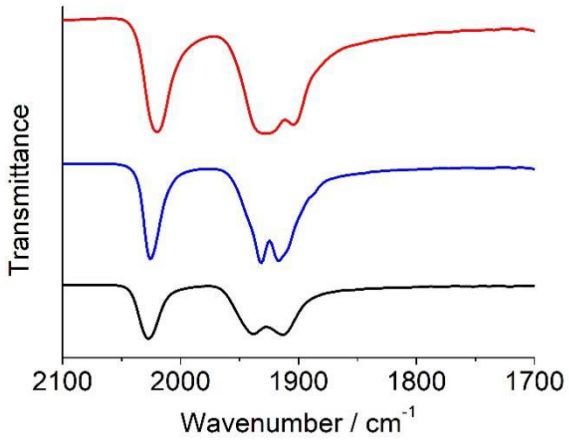

Figure S 10 Experimental FTIR spectra of **1p**(red line) , **2p**(blue line) and **3**(black line) recorded in KBr displaying characteristic $\boldsymbol{v_{CO}}$ stretching modes for their facial tricarbonyl geometries.

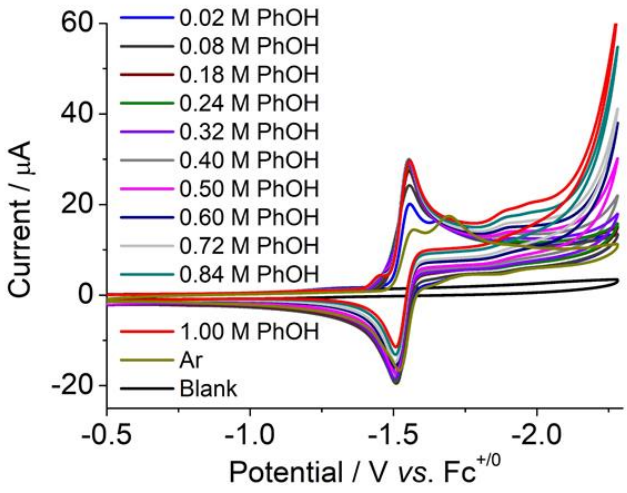

Figure S 11 CVs of 0.5 mM **1p** with varied concentrations of phenol under Ar. Voltammograms are taken at a scan rate of 100 mV/s with 0.1 M $^{n}Bu_4NPF_6$ in MeCN solution. Glassy carbon working electrode, Ag^{+}/Ag reference electrode, and Pt wire counter electrode.

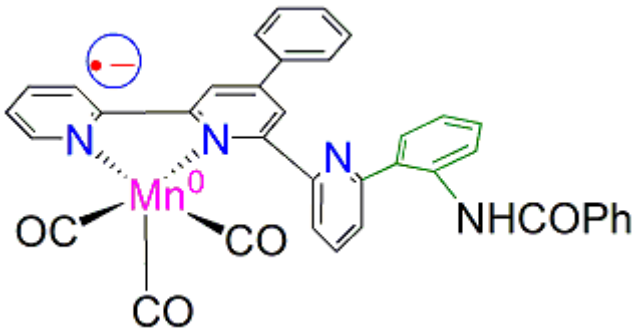

Figure S 12 Proposed structure of the intermediate [$\mathbf{1p}^{2-}$ - Br^-]

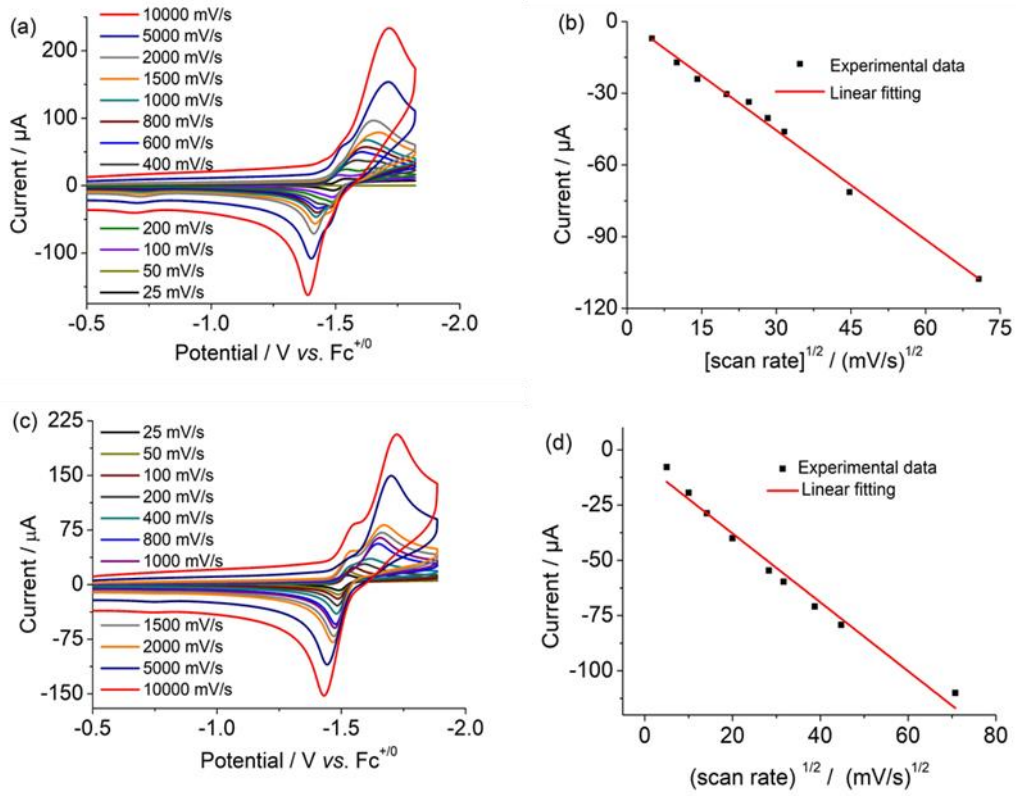

Figure S 13 (a) CVs of complex **1p** (0.5 mM) with scan rate (v) varied from 0.025 V/s to 10 V/s under Ar. (b) Plot of anodic peak current (i_p) vs. $v^{1/2}$ for complex **1p**. (c) Cyclic voltammograms of complex **2p** (0.5 mM) with scan rate (v) varied from 0.025 V/s to 10 V/s under Ar. (d) Plot of anodic peak current (i_p) vs. $v^{1/2}$ for complex **2p**. Voltammograms are taken in MeCN solution with 0.1 M ^{n}Bu$_4$NPF$_6$ as support electrolyte. Glassy carbon working electrode, Ag^+/Ag reference electrode, and Pt wire counter electrode.

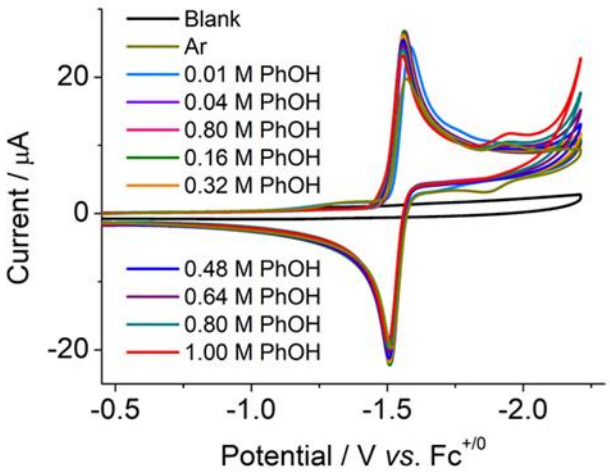

Figure S 14 CVs of 0.5 mM **2p** with varied concentrations of phenol under Ar. Voltammograms are taken at a scan rate of 100 mV/s with 0.1 M $^{n}Bu_4NPF_6$ in MeCN solution. Glassy carbon working electrode, Ag^{+}/Ag reference electrode, and Pt wire counter electrode.

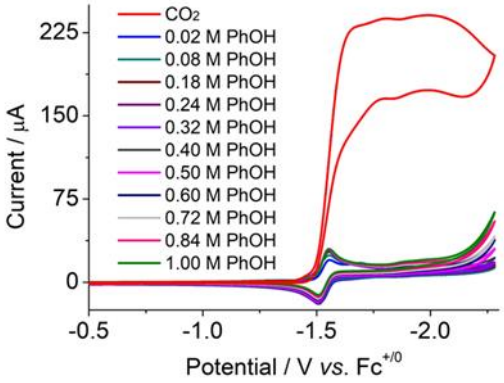

Figure S 15 CVs show 0.5 mM **1p** with varied amounts of phenol under Ar, and saturating with CO_2 in the presence of 1 M phenol. Voltammograms are taken at a scan rate of 100 mV/s with 0.1 M $^{n}Bu_4NPF_6$ in MeCN solution. Glassy carbon working electrode, Ag^{+}/Ag reference electrode, and Pt wire counter electrode.

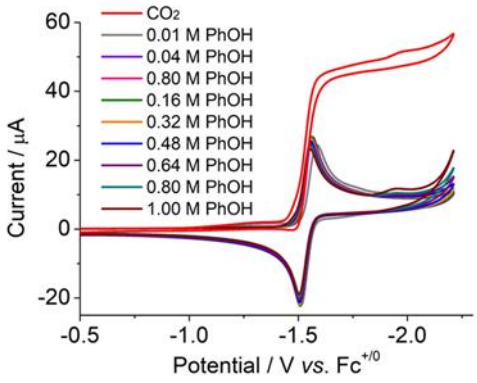

Figure S 16 CVs show 0.5 mM **2p** with varied amounts of phenol under Ar, and saturating with CO_2 in the presence of 1 M phenol. Voltammograms are taken at a scan rate of 100 mV/s with 0.1 M $^{n}Bu_4NPF_6$ in MeCN solution. Glassy carbon working electrode, Ag^+/Ag reference electrode, and Pt wire counter electrode.

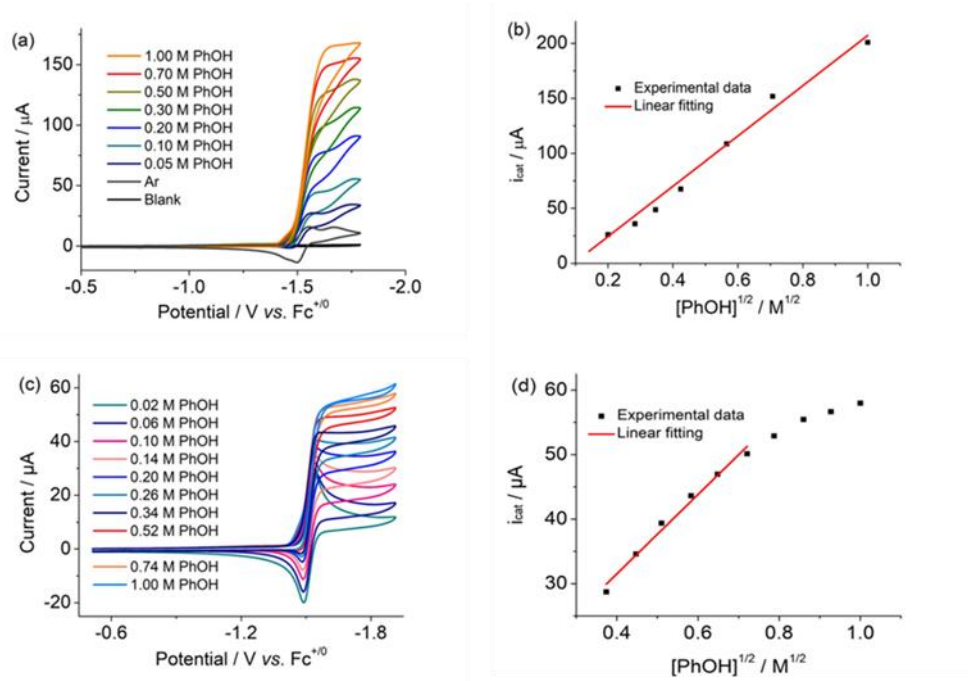

Figure S 17 (a) CVs show 0.5 mM **1p** with varied amounts of PhOH under CO_2. (b) The linear dependence of catalytic Current (i_{cat}) on the square root of the concentration of PhOH. (c) Cyclic voltammograms show 0.5 mM **2p** with varied amounts of PhOH under CO_2. (d) The linear dependence of catalytic Current (i_{cat}) on the square root of the concentration of PhOH. Voltammograms are taken at a scan rate of 100 mV/s with 0.1 M $^{n}Bu_4NPF_6$ in MeCN solution. Glassy carbon working electrode, Ag^+/Ag reference electrode, and Pt wire counter electrode.

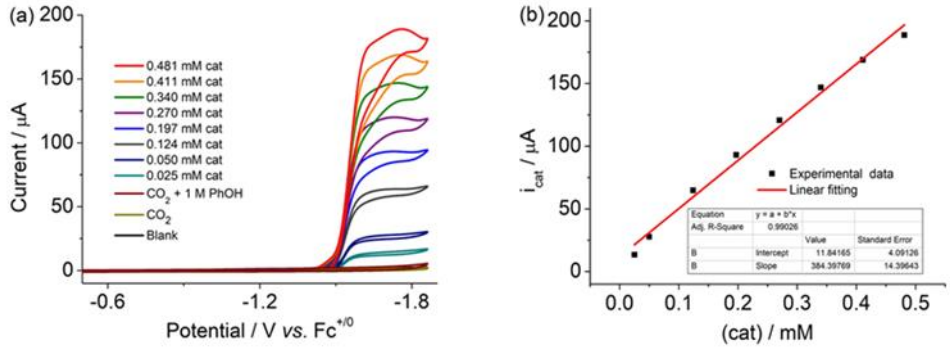

Figure S 18 (a) CVs of **1p** (0–0.481 mM) in the presence of 1 M PhOH under CO_2. (b) The linear dependence of catalytic Current (i_{cat}) on the concentration of the catalyst. Voltammograms are taken at a scan rate of 100 mV/s with 0.1 M $^{n}Bu_4NPF_6$ in MeCN solution. Glassy carbon working electrode, Ag^+/Ag reference electrode, and Pt wire counter electrode

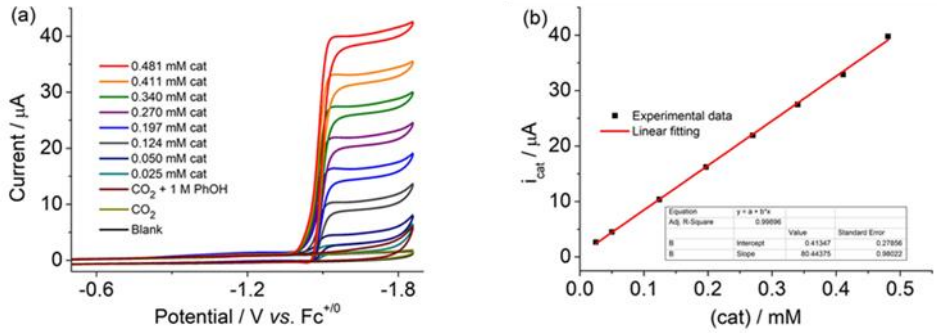

Figure S 19 (a) CVs of **2p** (0–0.481 mM) in the presence of 1 M PhOH under CO_2. (b) The linear dependence of catalytic Current (i_{cat}) on the concentration of the catalyst. Voltammograms are taken at a scan rate of 100 mV/s with 0.1 M $^{n}Bu_4NPF_6$ in MeCN solution. Glassy carbon working electrode, Ag^+/Ag reference electrode, and Pt wire counter electrode.

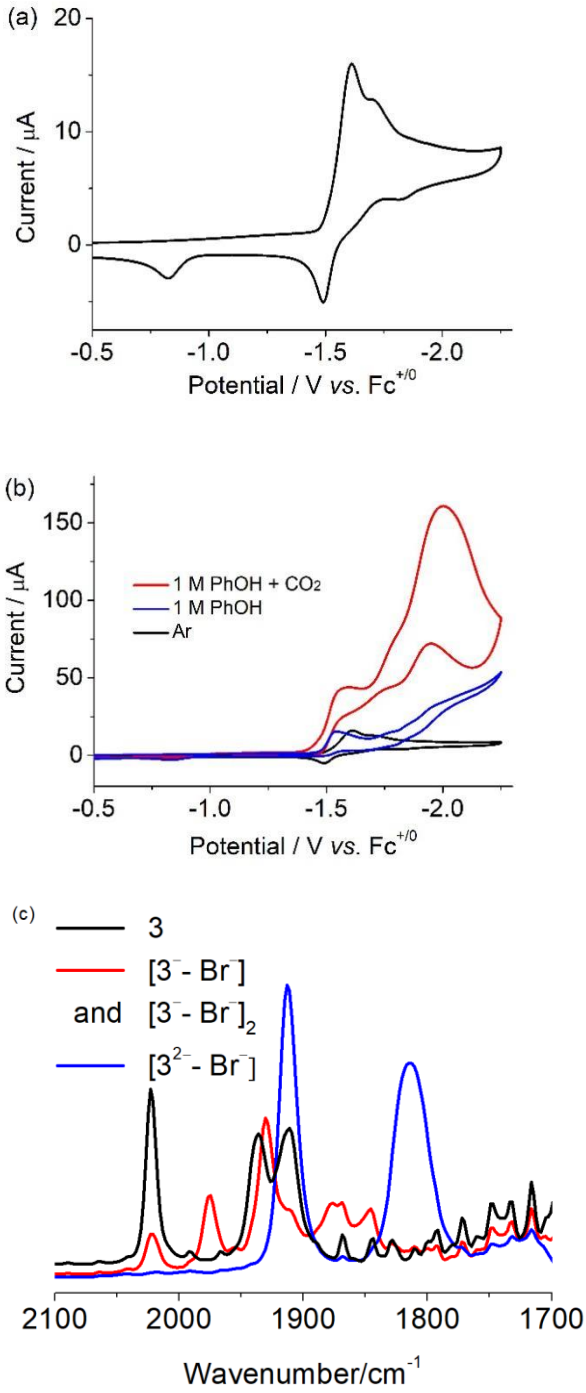

Figure S 20 (a) Cyclic voltammogram show **3** (0.5 mM) under Ar with a scan rate of 100 mV/s. (b) CVs of 0.5 mM **3** under Ar (black), in the presence of 1 mM phenol (blue) and saturated with CO_2 in the presence of 1 M phenol (red). Voltammograms are taken at a scan rate of 100 mV/s with 0.1 M $^{n}Bu_4NPF_6$ in MeCN solution. Glassy carbon working electrode, Ag^+/Ag reference electrode, and Pt wire counter electrode. (c) IR-SEC of a 1mM solution of **3** in MeCN under Ar. Reduction at the potential corresponding to the first peak current.

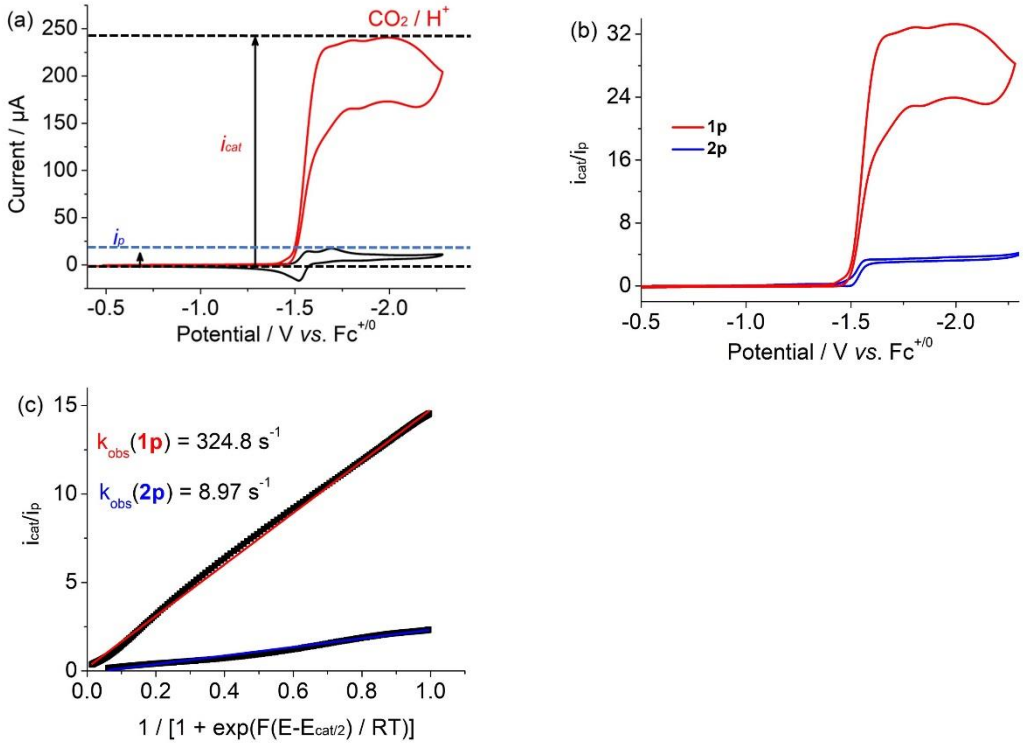

Figure S 21 (a) CVs of 0.5 mM **1p** under Ar in the absence of phenol (black line), under CO_2 in the presence of 1 M phenol (red line). Voltammograms are taken at a scan rate of 100 mV/s with 0.1 M $^{n}Bu_4NPF_6$ in MeCN solution. (b) Cyclic voltammetry of **1p** (red line) and **2p** (blue line) in the potential domain of the catalytic CO_2 reduction wave in acetonitrile + 0.1 M $^{n}Bu_4NPF_6$ + 1 M PhOH, at 0.1 V/s under 1 atm. CO_2 (catalyst concentration is 0.5 mM). The current, i_{cat} is normalized against the peak current of the reversible one-electron reversible wave, i_p obtained at the same scan rate (0.1 V/s). (c) Foot-of-the-wave analysis of **1p** and **2p** under equivalent experimental conditions with a linear fit extrapolated from ($E - E_{cat}$) at a scan rates of 0.1 V/s.

Details for Foot-of-the-Wave Analysis (FOWA) and determination of k_{obs}.

Foot-of-the-Wave Analysis was applied to cyclic voltammetry measurements as described by Savéant and coworkers (*Science*, **2012**, *338 (6103)*, 90-94;) in order to determine k_{obs} = TOF under the specified conditions. At the outset of each experiment, a cyclic voltammogram was measured of catalyst alone under inert atmosphere in the presence of proton source, from which E^0_{cat} could be determined. The half of the peak height of the formal **1p**/(**1p**$^{2-}$ - Br^-) couple, i^0_p, was determined by taking the difference between peak cathodic current and baseline current before this couple.

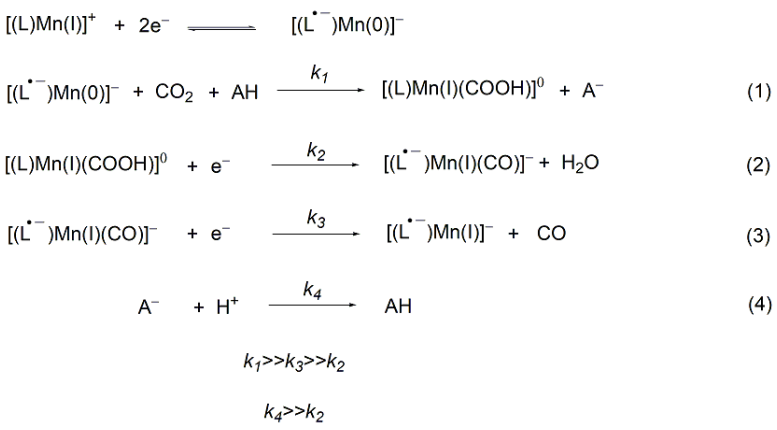

The rate-determine step (2) for CO_2 reduction with complex **1p** (or **2p**) may be described as an EC process, involving one electron transfer followed by C-OH bond cleavage. The following relationship may be derived:

$$\frac{i}{i_p^0} = \frac{2.24\sqrt{\frac{k_{obs}}{fv}}}{1 + e^{[f(E-E_{cat}^0)]}}$$

where i is the catalytic current, E is the potential, v is the scan rate (V/s), k_{obs} is the observed rate constant, and f = F/RT = 38.94 V^{-1}. Thus, a "FOW" plot of $\frac{i}{i_p^0}$ *versus* $\frac{1}{1+e^{[f(E-E_{cat}^0)]}}$ yields a straight line with slope $2.24\sqrt{\frac{k_{obs}}{fv}}$, from which k_{obs} may be determined.

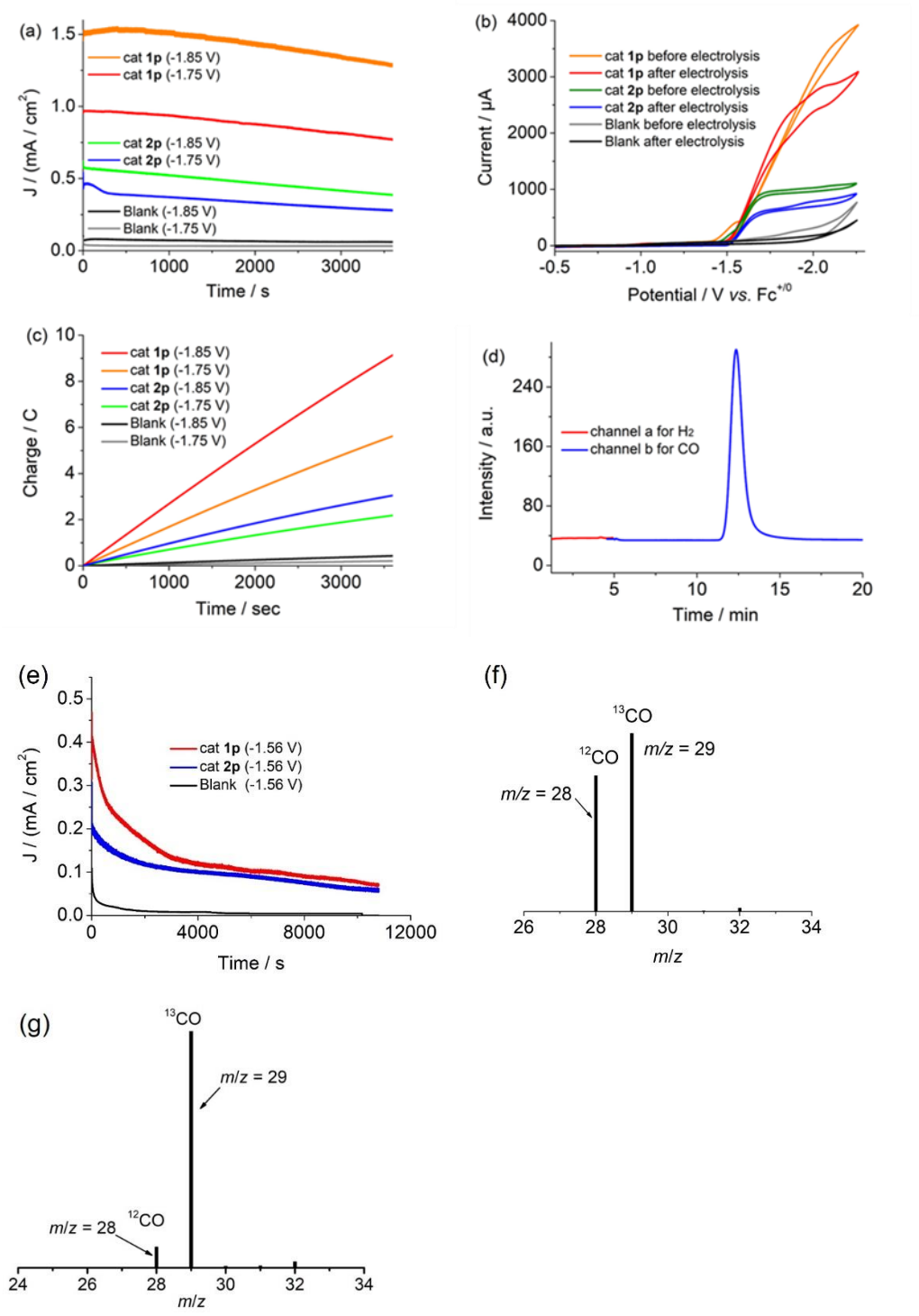

Figure S 22 (a) Controlled potential electrolysis at -1.75 V and -1.85 V *vs.* $Fc^{+/0}$ in the presence and absence of 0.5 mM **1p** (or **2p**) under CO_2 in the presence of 1 M phenol. (b) Cyclic voltammograms show 0.5 mM **1p** and **2p** before and after electrolysis at -1.85 V *vs.* $Fc^{+/0}$ under CO_2 in the presence of 1 M phenol. (c) The charge integration after electrolysis for **1p** and **2p** (d) The gas products channel of **1p**. (e) Controlled potential electrolysis at -1.56 V *vs.* $Fc^{+/0}$ under CO_2 in the presence of

1 M phenol in the presence and absence of 0.5 mM **1p** (or **2p**). (f) Mass spectrum of the gaseous phase resulting from electrolysis of the $^{13}CO_2$ saturated solution containing 0.5 mM **1p** at −1.85 V over 0.5 h and (g) 1 h. Conditions: 0.1 M $TBAPF_6$ in CH_3CN with 1 M phenol, glassy carbon working electrode, graphite rod counter electrode, Ag^+/Ag reference electrode. Voltammograms are taken at a scan rate of 100 mV/s with 0.1 M $^nBu_4NPF_6$ in MeCN solution. Glassy carbon working electrode, Ag^+/Ag reference electrode, and Pt wire counter electrode.

Detail discussion in comparable **controlled potential electrolysis (CPE)** results of complexes **1p** and **2p**

Comparable controlled potential electrolysis (CPE) studies of complexes **1p** and **2p** were explored under CO_2 atmosphere in the presence of 1.0 M phenol at varied potentials with a custom cell designed in our laboratory. At an applied potential of – 1.85 V, an average electrocatalytic current of 1.4 mA/cm^2 was observed for **1p** in a period of 1 h (Figures S21). CVs following the electrolysis indicated a slight decay in the amplitude of catalytic current (Figures S22), consistent with the observation that a decrease in the catalytic current during CPE. Since the formation of catalytic active nanoparticles were excluded by the negligible current observed after a "rinse test" following CPE, the current decay was assumed to be a result of catalyst decomposition. Analysis of the gas mixture in the headspace of the working compartment by GC confirmed CO as the main production and a trace amount of H_2. Analysis of the liquid phase by ion chromatography detected no other transformed product. In addition, negligible CO amounts were found in the headspace of the counter electrode compartment. Control experiments showed that only negligible current densities and trace amount of CO were produced in the absence of **1** (Figure S22). Finally, a total *Faradaic Efficiency* (*FE*) for CO and H_2 of 100 ± 2% and a *Turnover Numbers* (*TON*, mol ($CO+H_2$)/mol cat) of 11.83 based on **1p** were obtained (Table S5). At the same cathodic applied potential, complex **2p** only produced a low current of 0.3 mA/cm^2 with the *TON* value for CO production sharply decreasing to 2.1 (Figure S22). The electrocatalytic properties of **1p** and **2p** summarized in table S5 indicates a notable effect of the proton tunneling distance on CO_2 reduction. Controlled potential electrolysis at –1.56 V (Figure S22e), neither the charge nor the TON for both

complexes is significantly lower than that at –1.85 V, owing to the weaker driving force for electrochemical reduction of CO_2. Isotope labelling experiment with $^{13}CO_2$ is really hard to exclude the carbon source of CO is CO_2 (Figure S22f), especially for a system which might release CO from itself. However, extend the electrolysis time would lead to obviously increase in the ratio of ^{13}CO (Figure S22g), support the conversion of CO_2 to CO.

Table S 4 Quantitative analysis of the CPE results of **1p** and **2p**

Complex	**1p**	**1p**	**1p**	**2p**	**2p**	**2p**	Blank	Blank	Blank
Proton source (1 M)	PhOH	PhOH	PhOH	PhOH	PhOH	PhOH	PhOH	PhOH	PhOH
Potential/V *vs.* $Fc^{+/0}$	-1.85	-1.75	-1.56	-1.85	-1.75	-1.56	-1.85	-1.75	-1.56
Q / C	9.135	5.622	1.412	3.049	2.184	1.046	0.427	0.207	0.088
n_{H2} : n_{CO}	1.3: 99.2	0.7:99.5	0.9: 138	0 : 100	0.3 : 99.5	1.4 : 110	4.2 : 0	12.5 : 0	0
TON	11.83	2.1	1.45	2.5	1.73	0.49	/	/	/
Faradaic efficiencies	95.3	96.3	93.7	85.9	90.5	91.6			

Table S 5 Comparison of the electrocatalytic properties of complex **1p**, **2p**.

Complex	Proton source (1 M)	$E_{1/2}$(V) *vs.* $Fc^{+/0}$	i_{cat}/i_p	$TOF_{max}(s^{-1})$	η(V) *vs.* $Fc^{+/0}$	TON
1p	PhOH	-1.56	16.6	325	0.21	10
2p	PhOH	-1.52	1.7	9 [a]/10.48[b]	0.17	2

a, obtained by foot-of-the-wave analysis (FOWA). b, obtained by the catalytic plateau current analysis.

11. DFT Calculations

Computational Details.

All geometry optimizations were obtained from density functional theory with the M06 exchange-correlation functional[1] computations as implemented in Gaussian 09[2]. Nonmetals (C, H, O, N) used 6-31G(d,p) basis set[3, 4] and SDD[5] was used for Mn. The single point energies of optimized structures were calculated at M06/[6-311++G(d,p) + SDD] level. Harmonic vibrational frequencies were computed at the same level to obtain the entropic corrections and to verify the nature of stationary points. All geometric structure optimizations, vibrational frequency calculations and single point energy calculations were obtained in acetonitrile solvent using the polarizable continuum model (CPCM)[6,7]. The effectiveness of our computatioal method has been demonstrated by our previous studies to successfully reproduce the experimental reduction potentials and CO stretching bands.[8-10]

The reduction potential $E_{O|R}$ relative to the ferrocene/ferrocenium couple was calculated using the following formula:

$$E_{O|R} = -\frac{\Delta G_{O|R}}{nF} - E_{SCE}^{ref} - 0.384V$$

ΔG is the total Gibbs free energy; n is the number of electrons involved in the electrochemistry reaction. F is Faraday's constant. $E_{SCE}^{ref}$is taken as -4.422 V[11], which is the absolute potential of saturated calomel electrode (SCE) in acetonitrile solution. -0.384 V is the shift value of reduction potential for ferrocene/ferrocenium couple relative to SCE.[12] For the reactions involving the participation of electrons, the energy contributions due to the negative reductive potential were added to all the species after each electronreduction step.

Refs

[1] Zhao, Y.; Truhlar, D. G. The M06 suite of density functionals for main group thermochemistry, thermochemical kinetics, noncovalent interactions, excited states, and transition elements: two new functionals and systematic testing of four M06-class functionals and 12 other functionals.

Theor. Chem. Acc. **2008**, 120, 215-241.

[2] Frisch, M. J.; Trucks, G. W.; Schlegel, H. B.; Scuseria, G. E.; Robb, M. A.; Cheeseman, J. R.; Scalmani, G.; Barone, V.; Mennucci, B.; Petersson, G. A.; Nakatsuji, H.; Caricato, M.; Li, X.; Hratchian, H. P.; Izmaylov, A. F.; Bloino, J.; Zheng, G.; Sonnenberg, J. L.; Hada, M.; Ehara, M.; Toyota, K.; Fukuda, R.; Hasegawa, J.; Ishida, M.; Nakajima, T.; Honda, Y.; Kitao, O.; Nakai, H.; Vreven, T.; Montgomery, J. J. A.; Peralta, J. E.; Ogliaro, F.; Bearpark, M.; Heyd, J. J.; Brothers, E.; Kudin, K. N.; Staroverov, V. N.; Kobayashi, R.; Normand, J.; Raghavachari, K.; Rendell, A.; Burant, J. C.; Iyengar, S. S.; Tomasi, J.; Cossi, M.; Rega, N.; Millam, J. M.; Klene, M.; Knox, J. E.; Cross, J. B.; Bakken, V.; Adamo, C.; Jaramillo, J.; Gomperts, R.; Stratmann, R. E.; Yazyev, O.; Austin, A. J.; Cammi, R.; Pomelli, C.; Ochterski, J. W.; Martin, R. L.; Morokuma, K.; Zakrzewski, V. G.; Voth, G. A.; Salvador, P.; Dannenberg, J. J.; Dapprich, S.; Daniels, A. D.; Farkas; Foresman, J. B.; Ortiz, J. V.; Cioslowski, J.; Fox, D. J. Gaussian 09, Revision D.01; Gaussian, Inc.: Wallingford, CT, **2009**.

[3] Hehre, W. J.; Ditchfield, R.; Pople, J. A. Self-consistent molecular orbital methods. XII. Further extensions of gaussian-type basis sets for use in molecular orbital studies of organic molecules. *J. Chem. Phys.* **1972**, 56, 2257-2261.

[4] Hariharan, P. C.; Pople, J. A. The influence of polarization functions on molecular orbital hydrogenation energies. *Theor. Chim. Acta.* **1973**, 28, 213-222.

[5] Dolg M.; Wedig U.; Stoll H.; Preuss H. Energy-adjusted ab initio pseudopotentials for the first row transition elements. *J. Chem. Phys.* **1987**, 86, 866-872.

[6] Barone V.; Cossi M. Quantum calculation of molecular energies and energy gradients in solution by a conductor solvent model. *J. Phys. Chem. A* **1998**, 102, 1995-2001.

[7] Cossi M.; Rega N.; Scalmani G.; Barone V. Energies, structures, and electronic properties of molecules in solution with the C-PCM solvation model. *J. Comp. Chem.* **2003**, 24, 669-681.

[8] He S.; Huang F.; Wu Q.; Zhang P.; Xiong Y.; Yang J.; Zhang R.; Wang F.; Chen L.; Liu T. L.; Li F. Multiple-Site Concerted Proton-Electron Transfer in a ManganeseBased Complete Functional Model for [FeFe]-Hydrogenase. *Angew. Chem. Int. Ed.* **2021**, 60, 25839-25845.

[9] Yang J.; He S.; Wu Q.; Zhang P.; Chen L.;Huang F.; and Li F. A bio-inspired mononuclear manganese catalyst for high-rate electrochemical hydrogen production. *Dalton Trans.* **2021**, 50, 4783-4788.

[10] Wu Q.; Li M.; He S.; Xiong Y.; Zhang P.; Huang H.; Chen L.;Huang F.; and Li F. The hangman effect boosts hydrogen production by a manganese terpyridine complex. *Chem. Commun*. **2022**, 58, 5128-5131.

[11] Isse A. A.; Gennaro A. Absolute potential of the standard hydrogen electrode and the problem of interconversion of potentials in different solvents. *J. Phys. Chem. B* **2010**, 114, 7894-7899.

[12] Ngo K. T.; McKinnon M.; Mahanti B.; Narayanan R.; Grills D. C.; Ertem M. Z.; Rochford J. Turning on the protonation-first pathway for electrocatalytic CO_2 reduction by manganese bipyridyl tricarbonyl complexes. *J. Am. Chem. Soc.* **2017**, 139, 2604-2618.

Table S6 Selected experimental and calculated υ_{CO} for the proposed intermediates in pure MeCN

Complexes	Experimental / cm^{-1}	DFT / cm^{-1}
1	1927, 1856	1925, 1865,
[$\mathbf{1}^{2-}$-Br^-]	1841, 1777	1848, 1790
2	1927, 1856,	1923, 1865
[$\mathbf{2}^{2-}$-Br^-]	1841, 1777	1846, 1790

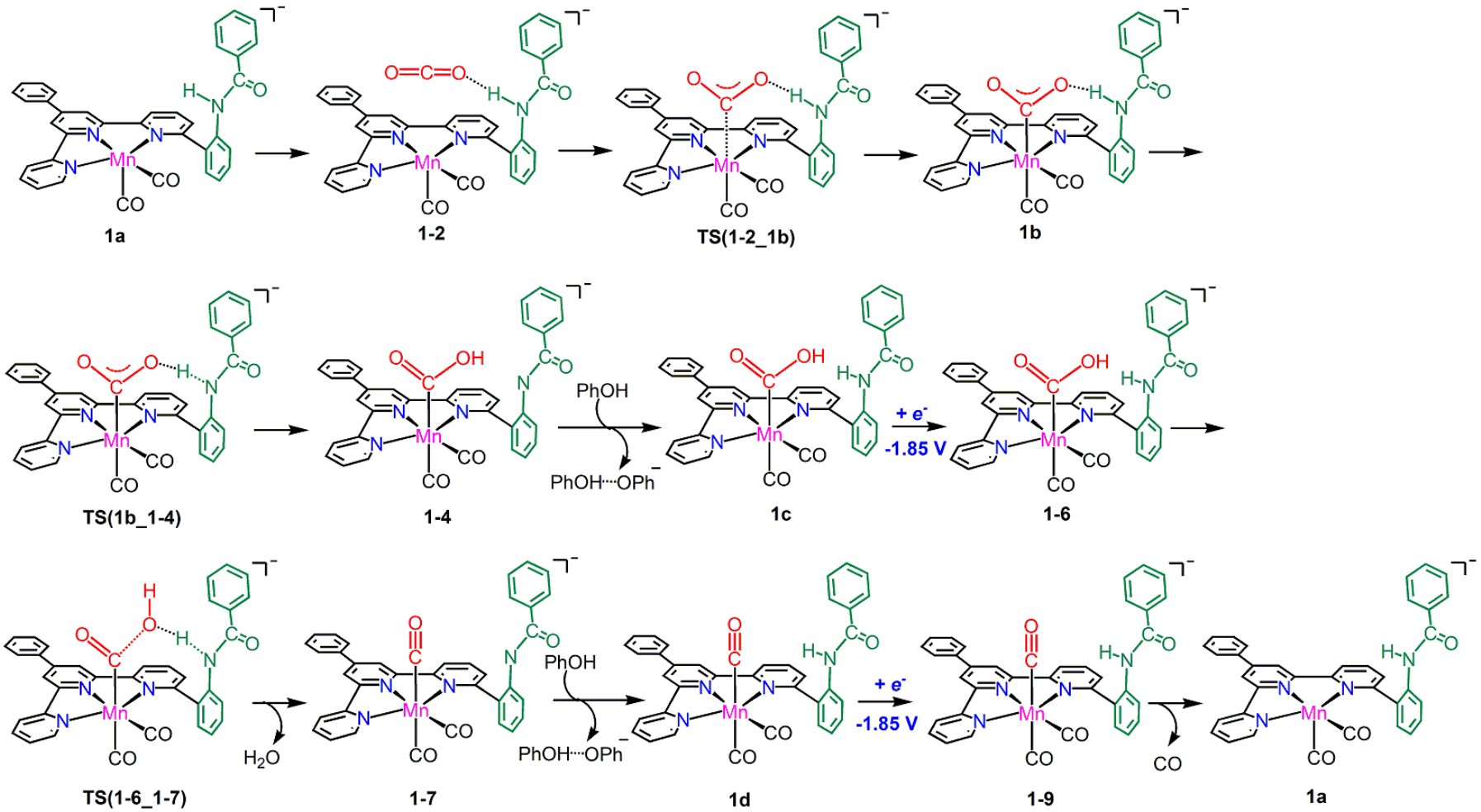

Scheme S 7 Speculative electrocatalytic cycle for the reduction of CO_2 to CO mediated by **[1^{2-}–Br$^-$]** **（1a）** or **[2^{2-}–Br$^-$]** **（2a）** at -1.85 V *vs* $Fc^{+/0}$.

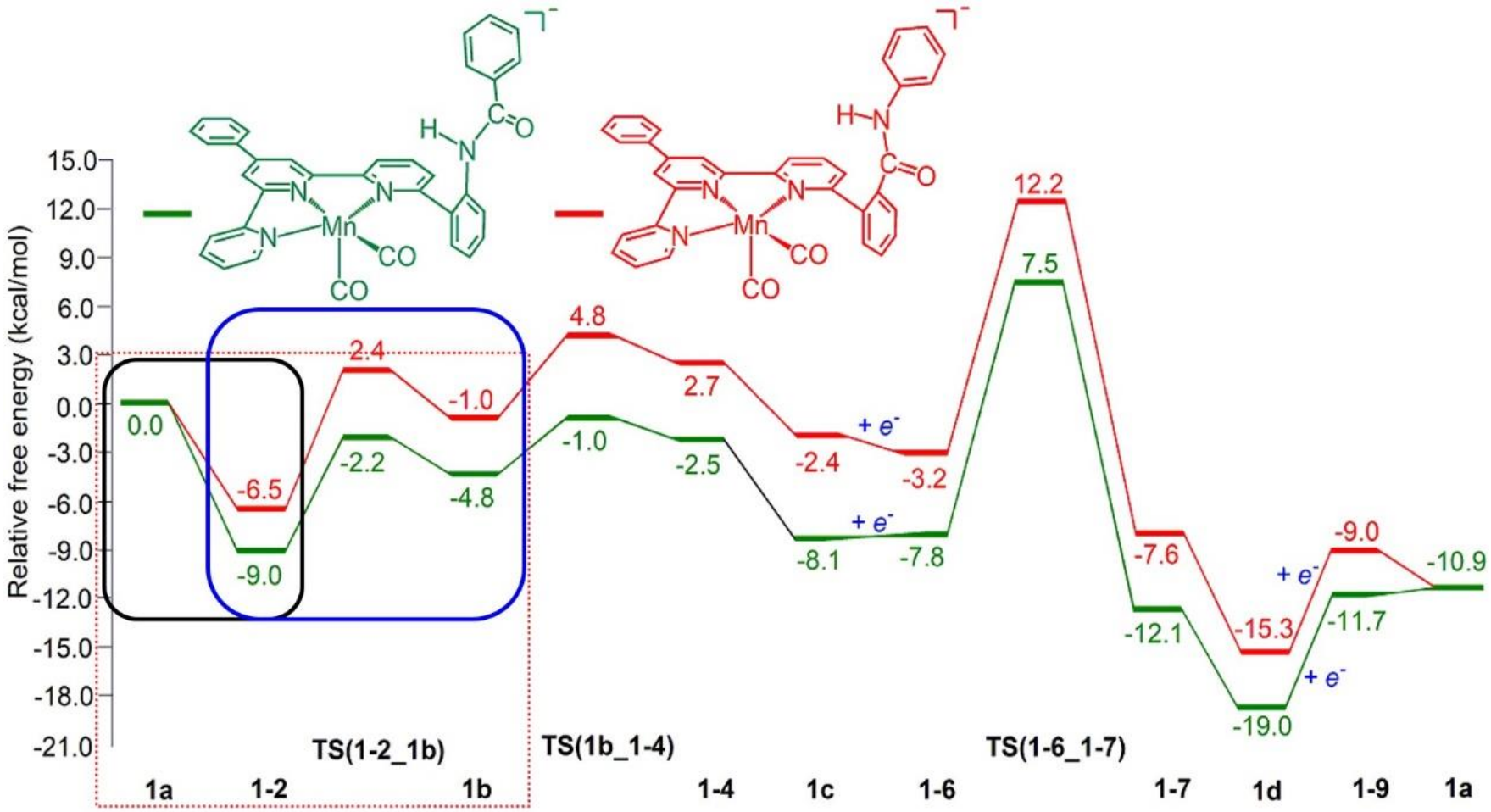

Figure S 23 Gibbs free energy (kcal mol^{-1}) profile for the electrochemical reduction of CO_2 to CO catalyzed by **1**(green line) or **2** (red line) at -1.85 V *vs* $Fc^{+/0}$.

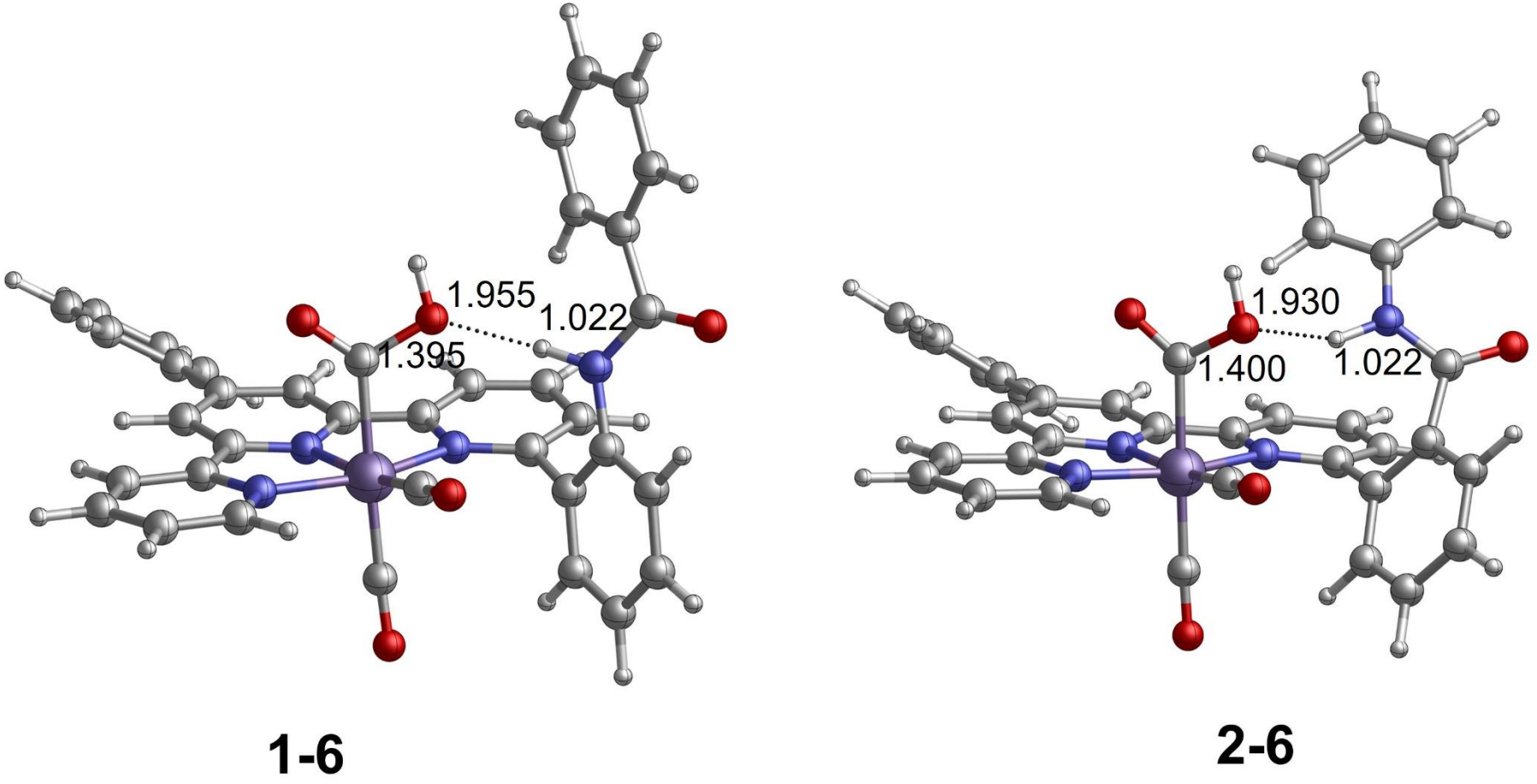

Figure S 24 Optimized geometries of **1-6** and **2-6** for the proton tunneling distance for C-OH bond cleavage. Bond lengths are shown in Angstroms.

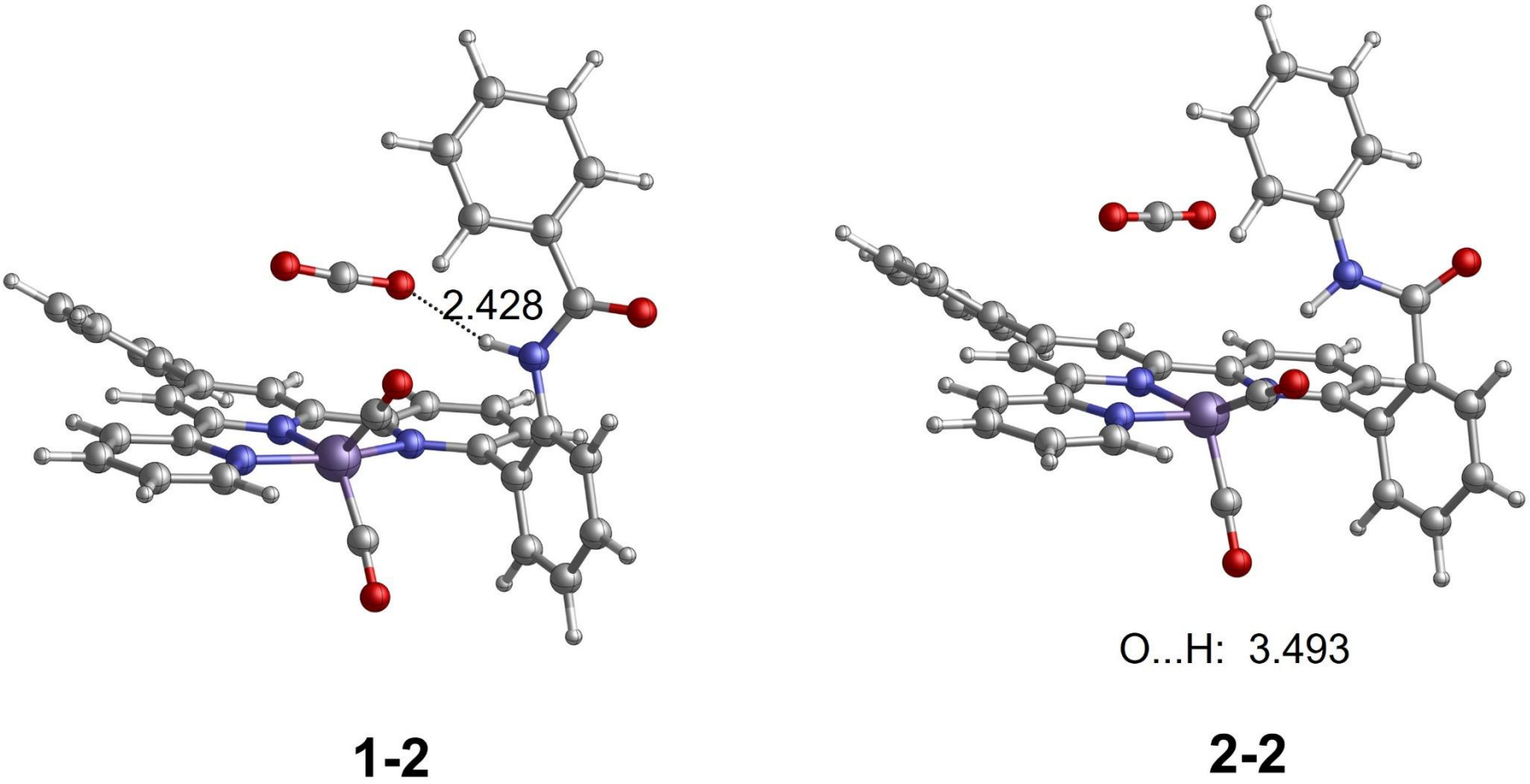

Figure S 25 Optimized geometries of **1-2** and **2-2** for the proton tunneling distance for CO_2 binding. Bond lengths are shown in Angstroms.

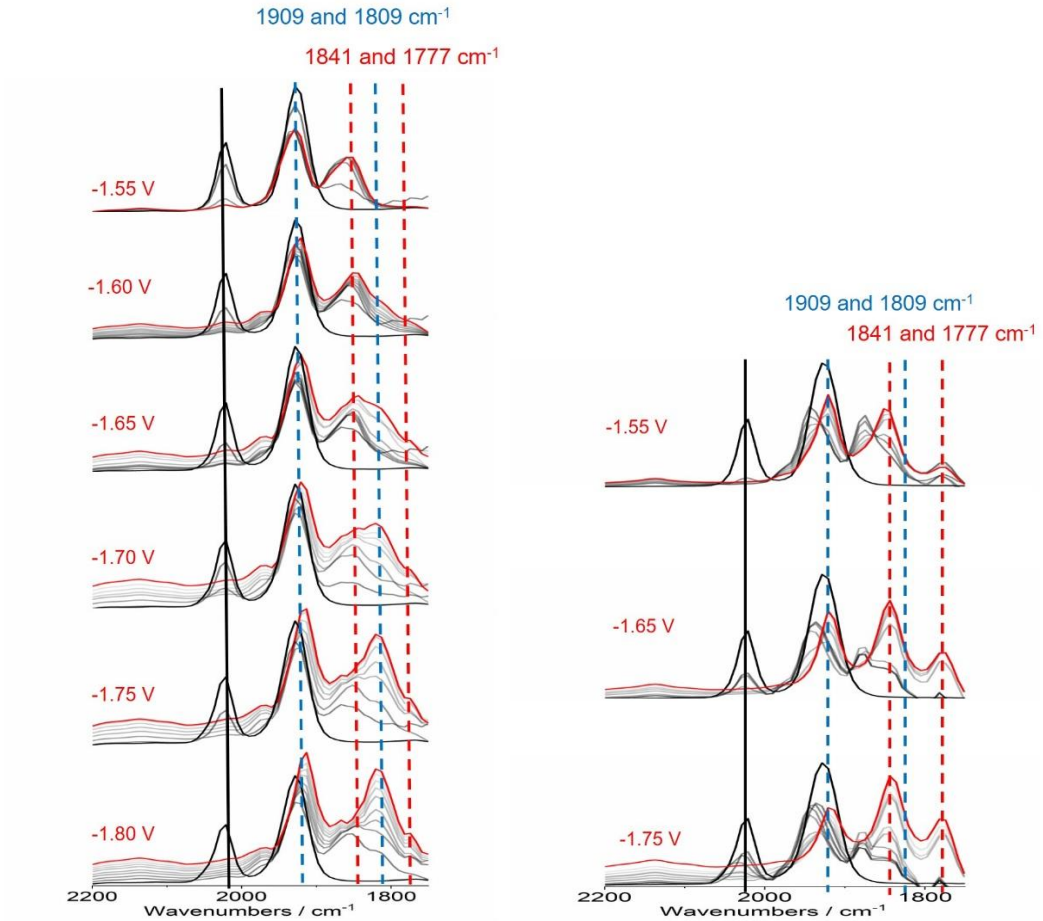

Figure S26 IR-SEC of 0.5 mM **1p** (left) and **2p** (left) in the presence of 0.5 M phenol under CO_2 atmosphere with varied electrolysis potential. The resting species **1p** (or **2p**) (black line), the final species after electrolysis at an applied electrolysis potential (red line).

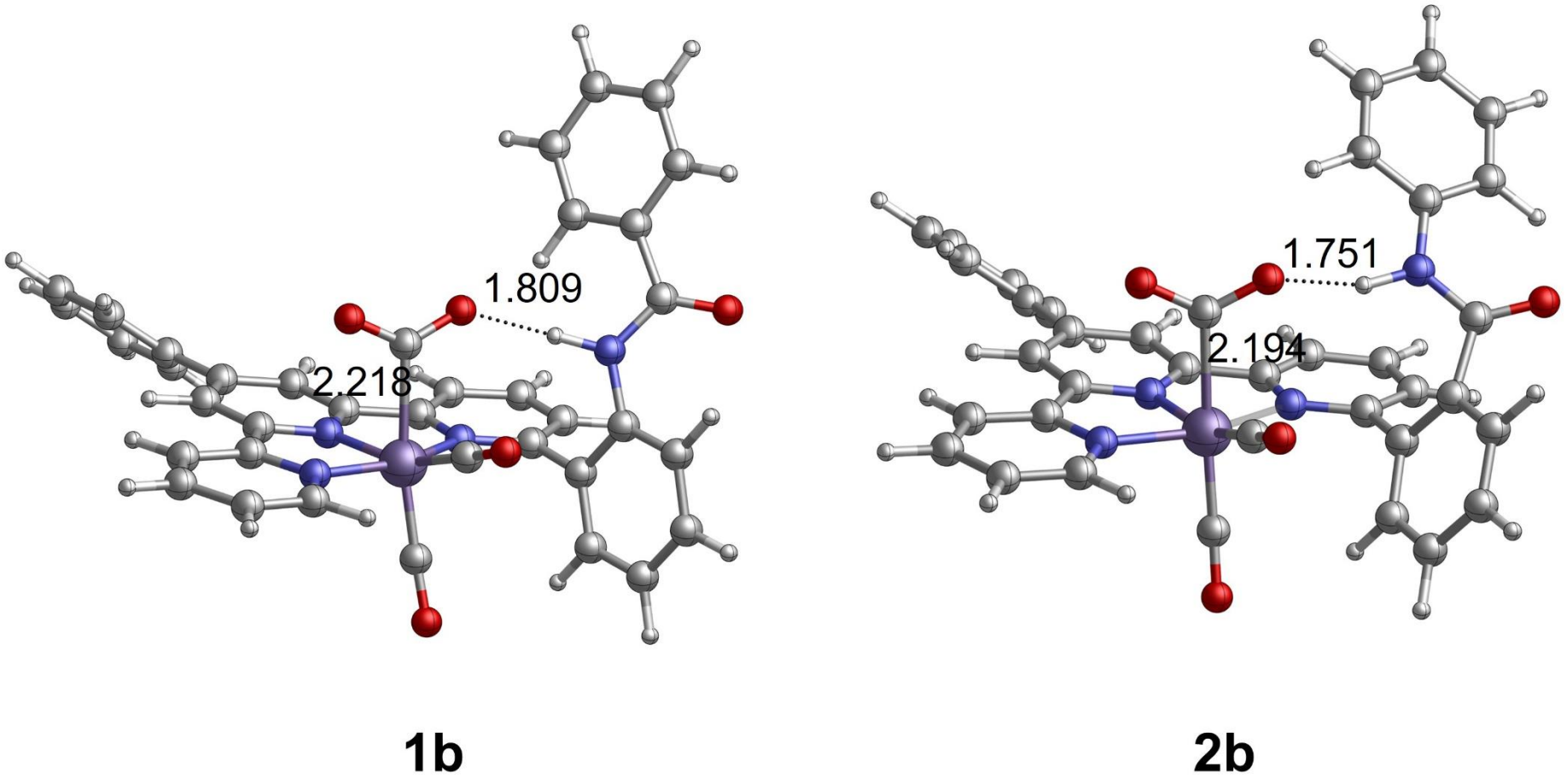

Figure S 27 Optimized geometries of **1b** and **2b** for the interaction of the bound CO_2 molecule with intramolecular amide. Bond lengths are shown in Angstroms.